Ioffe Institute Seminar

The effects of interfaces in the PIDT/BT-single walled carbon nanotube heterogeneous complexes on Multiple exciton generation

Baode Zhang

Liaoning Petrochemical University

19 May 2025 Saint Petersburg， Russia

Outline

- 1. Motivation of MEG (multiple exciton genreation) of quantun dot
- (1) Quantum dot solar cells; (2) quantum chips
- 2. Challenge of MEG of SWNT conjugated polymer as quantun dot: the competition between MEG and Auger recombination, which reduce the excitons
- 3. Our solution to MEG of SWNT quantun dot: tailoring the competetion by forming heterogeneous π complexes, Heterojunction of Conjugated polymer/carbon nanotube
- 3.1 Experimental Results
- 3.2 Therotical Results
- 4. Conclusion

1 Motivation

Advantage of MEG of quantum dot

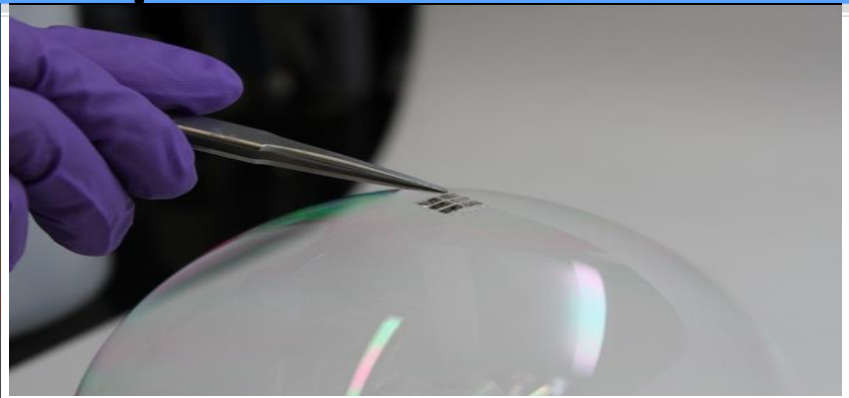

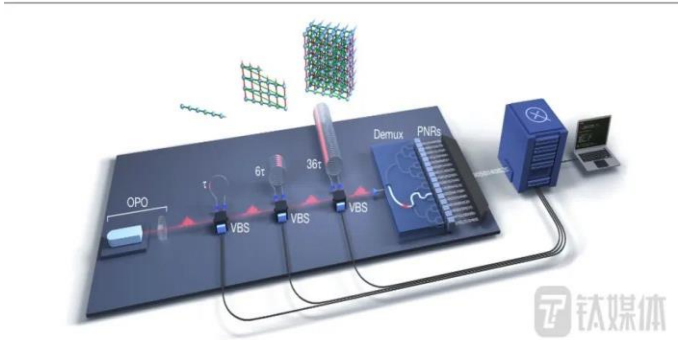

一、Application of quantum dots

1 solar cell

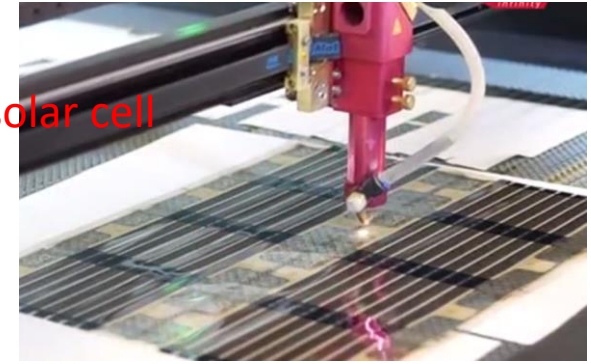

2 photon chip

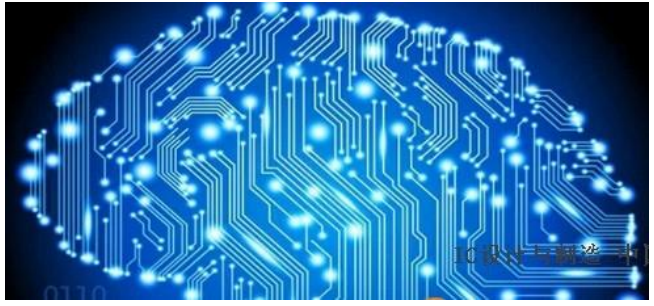

3 aerospace and astronautics

5 High-performance optoelectronic devices

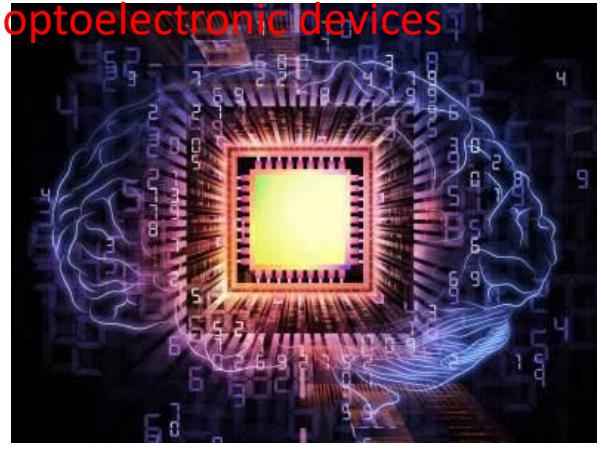

4 photonic quantum computer

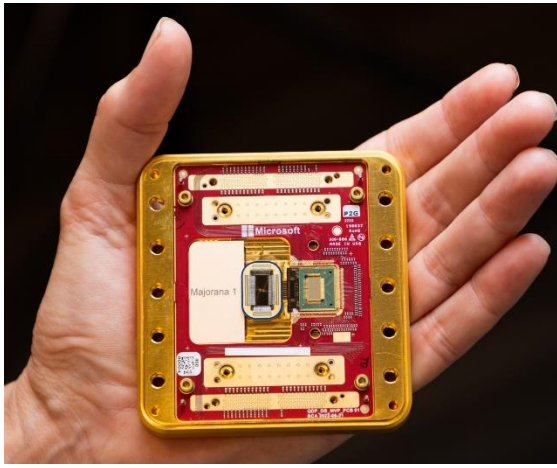

2023 Nobel prize winner to Quantum dot

AlexeiI.Ekimov

The concept of Quantum dot

1983 R. Rossetti, S. Nakahara, and L. E. Brus (*Bell Laboratories, Murray Hill, New Jersey 07974)and Ioffe physical technical Institue* ***Alexander Efros and Victor.I.Klimov*** *initiate the concept of colloidal quantun dot based on the quantum size effects of Cadmium Sulfide(CdS)*

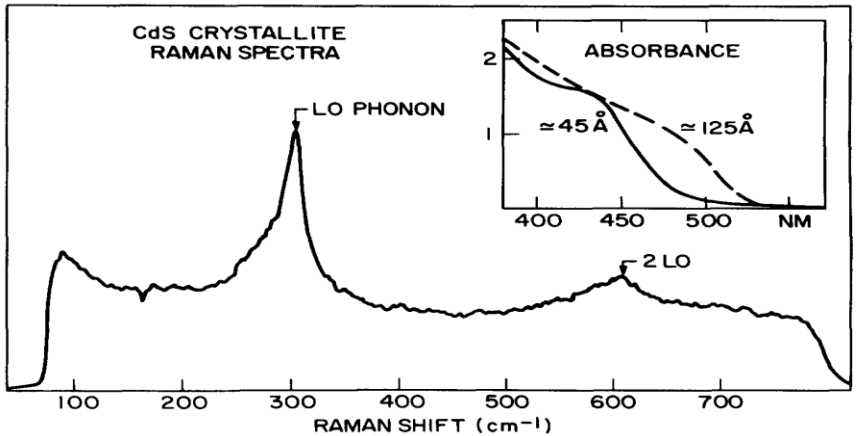

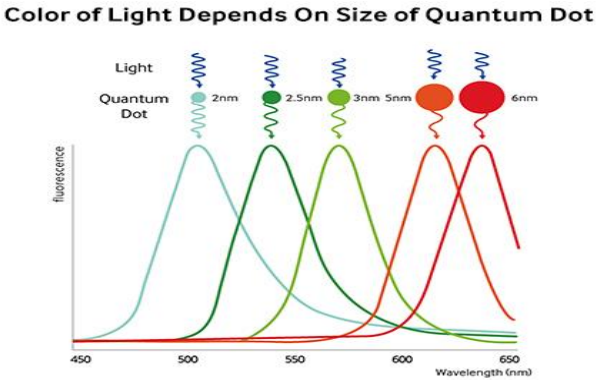

Quantum size effects in the redox potentials, resonance Raman spectra, and electronic spectra of CdS crystallites in aqueous solution. J. Chem. Phys. 1983, 79: 1086–1088.

In1993， Bawendi’ research group synthesis nearly monodisperse CdE (E = sulfur, selenium, tellurium) semiconductor nanocrystallites

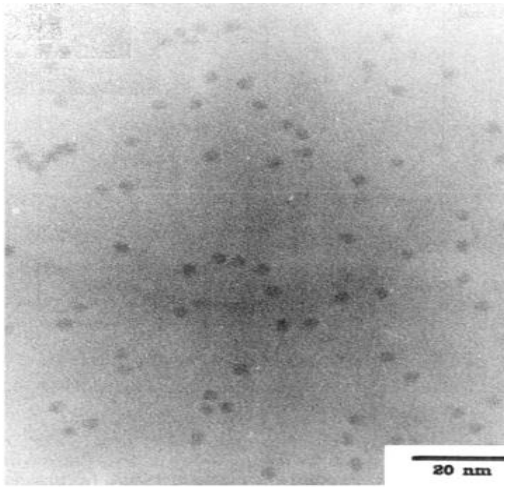

Figure 6. TEM image taken in bright field with lattice contrast
a collection of slightly prolate particles. The elongated (002) axis me
35.0 Å ± 5% while the perpendicular axis measures 30 Å ± 6%.
particles are well dispersed and not aggregated.

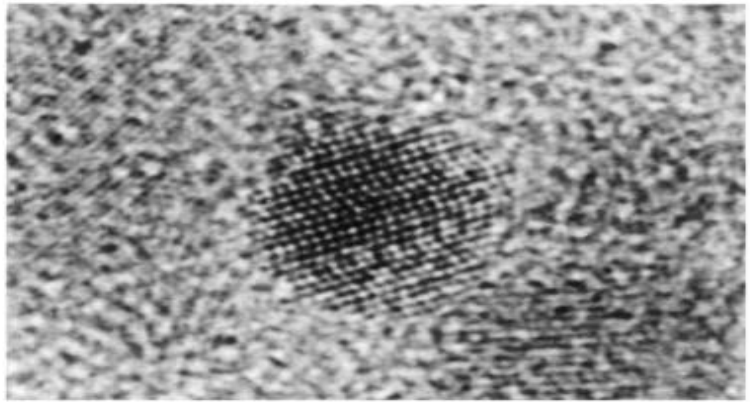

Figure 7. An 80 Å diameter CdSe crystallite imaged in bright field with
atom contrast shows the presence of stacking faults in the (002) direction.

Murray et al. Synthesis and characterization of nearly monodisperse CdE (E = sulfur, selenium, tellurium) semiconductor nanocrystallites. J. Am. Chem. Soc. 1993, **115**: 8706–8715.

Multiple Exciton Generation

1993, Landsberg, P., T., Nussbaumer, H., & G.Willeke reported the impact ionization, in which a high-energy electron of the conduction band makes a transition to a lower energy in the same band, as a result of a collision with an electron in the valence band. The latter is then promoted to the conduction band by gaining the energy lost by the first electron.The effect of impact ionization has been taken into account in the calculation of the maximum solar cell efficiency in the thermodynamic limit. A red shift of the optimum band gap is observed with respect to the Shockley-Queisser result. A maximum solar cell efficiency of 60.3% at E,=O.8 eV is predicted, which compares with 43.9% at Eg= 1.1 eV for the usual case.

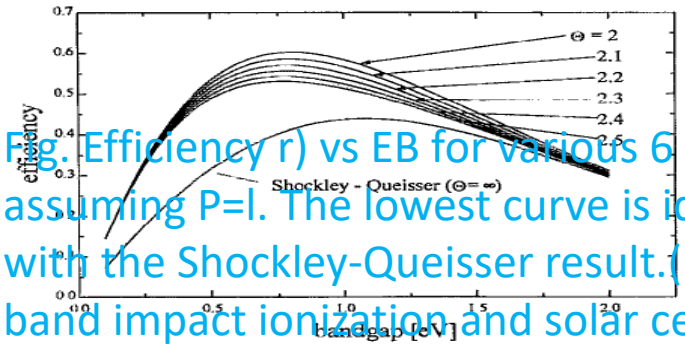

Fig. Efficiency r) vs EB for various 6 values, assuming P=l. The lowest curve is identical with the Shockley-Queisser result.(Ref. Band-band impact ionization and solar cell efficiency)

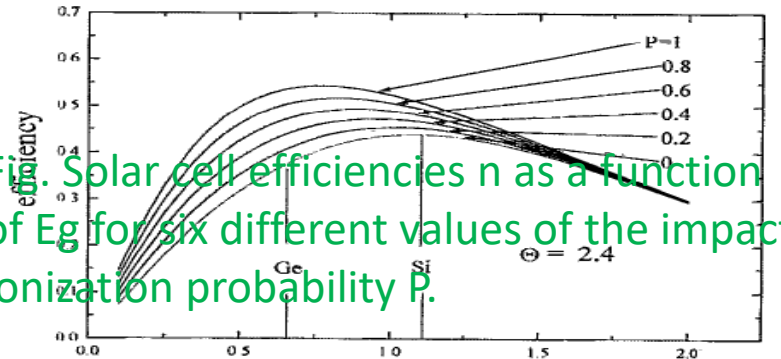

Fig. Solar cell efficiencies n as a function of Eg for six different values of the impact ionization probability P.

if impact ionization a

SWNT (single walled carbon nanotube) as quantum dot

(1) Quantum confinement and Enhanced Coulomb interactions

Quantum confinement of excitons and electrons in NCs and SWCNTs enhances dynamical exciton and electron-electron interactions, leading to many-body processes such as quantized Auger recombination (AR) and multiple exciton generation [(MEG) or carrier multiplication (CM)](Ref. Nozik, A. J.; Beard, M. C.; Luther, J. M.; Law, M.; Ellingson, R. J.; Johnson, J. C. Semiconductor quantum dots and quantum dot arrays and applications of multiple exciton generation to third-generation photovoltaic solar cells. Chem. Rev. 2010, 110, 6873–6890).

(2) Ensembles of the conduction band electrons and valence-band holes in semiconductors are complex systems that exhibit strong Coulomb interactions. Unique optical processes appear in these systems, owing to the presence of excitons, trions, biexcitons (excitonic molecules), bound exciton complexes, electronhole liquids, and electronhole plasmas.

The quantum effect of Semi-conductive Single wall carbon nanotube

Semiconducting nanocrystals (NCs) and single walled carbon nanotubes (SWCNTs) currently provide an excellent stage for experimental studies of the many body effects of electrons and excitons on optical processes in nanoscale materials

（ref．Klimov, V. I. Spectral and dynamical properties of multiexcitons in semiconductor nanocrystals. Annu. Rev. Phys. Chem. 2007, 58, 635–673; Kanemitsu, Y. Excitons in semiconducting carbon nanotubes: Diameter-dependent photoluminescence spectra. Phys. Chem. Chem. Phys. 2011, 13, 14879–14888）

Ref. Multiple Exciton Generation and Recombination in Carbon Nanotubes and Nanocrystals

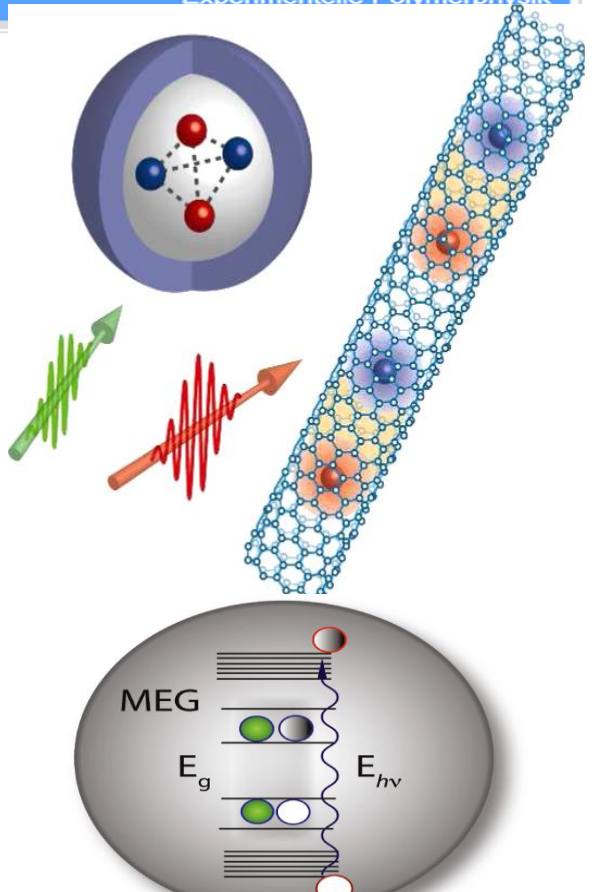

Single wall CNT as Quantum dot

- Higher photon-to-current conversion efficiencies than those defined by the Shockley-Quiesser limit of energy conversion

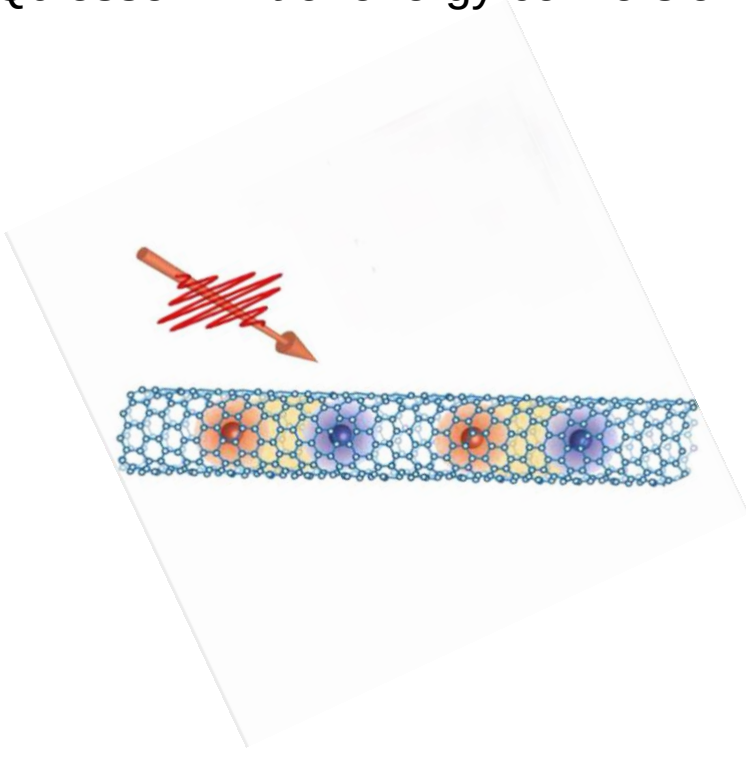

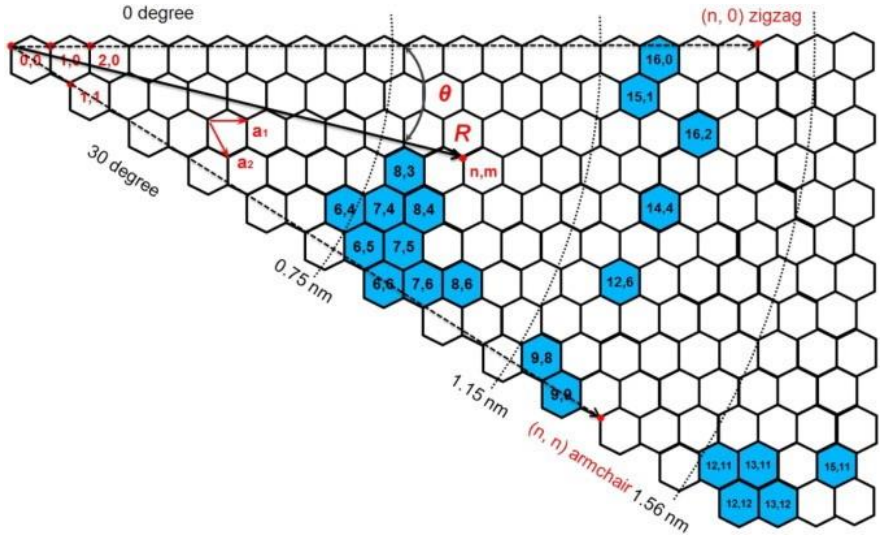

The possibility for Single walled carbon nanotube as quantum dots

1. Two dimensional quantum confinement of electrons and holes around the SWNT circumference leads to a distinctive density of states and well-defined selection rules for discrete optically allowed transitions.

2. SWNTs exhibit a strong Coloumb interaction between electons and holes(Many-electron effects often dramatically modify the properties of reduced dimensional systems. We report calculations, based on an ab initio many-electron Green's function approach, of electron-hole interaction effects on the optical spectra of small-diameter single-walled carbon nanotubes. Excitonic effects qualitatively alter the optical spectra of both semiconducting and metallic tubes. Excitons are bound by 1 eV in the semiconducting (8,0) tube and by 100 meV in the metallic (3,3) tube).(Ref. **Excitonic Effects and Optical Spectra of Single-Walled Carbon Nanotubes**)

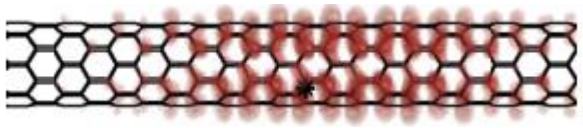

The 6.3 A° diameter semiconducting tube (8,0), in which we expect even larger excitonic effects. The

MEG of SWNT

The earliest report about multiple exciton generation of carbon nanotube can be traced back to Nobel prize winner Richard E. Smalley: “The observed nanotube fluorescence intensity was found to depend nonlinearly on the excitation intensity. this nonlinear behavior, which probably reflects annihilating interactions between multiple excitons on individual nanotubes.”(O'Connell M J , Bachilo S M , Huffman C B , et al. Band Gap Fluorescence from Individual Single-Walled Carbon Nanotubes[J]. Science, 2002,297(5581):593-596.)

Absorption of a single high energy photon can potentially create more than one charge carrier, whereby a highly energetic electron can lose excess energy by exciting a charge carrier across the energy gap

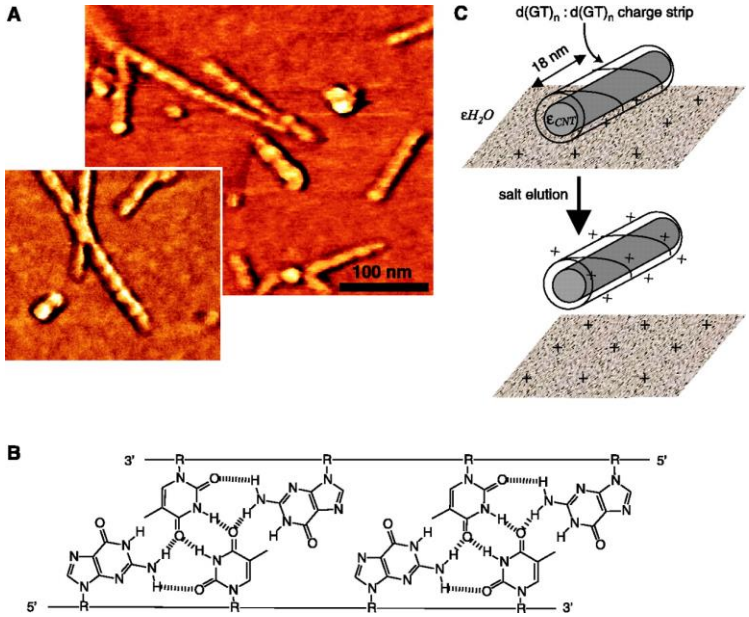

Mechanism of DNA-CNT separation. (A) AFM (phase image) of CNTs wrapped by d(GT)30, showing regular helical pitch of 18nm and height of 2 nm. (B) Proposed hydrogen-bonding interactions between two d(GT)n strands that lead to the formation of a "d(GT)n:d(GT)n charge strip." (C) Schematic for anion exchange separation process. At lower salt concentration, the surface-bound state is favored in

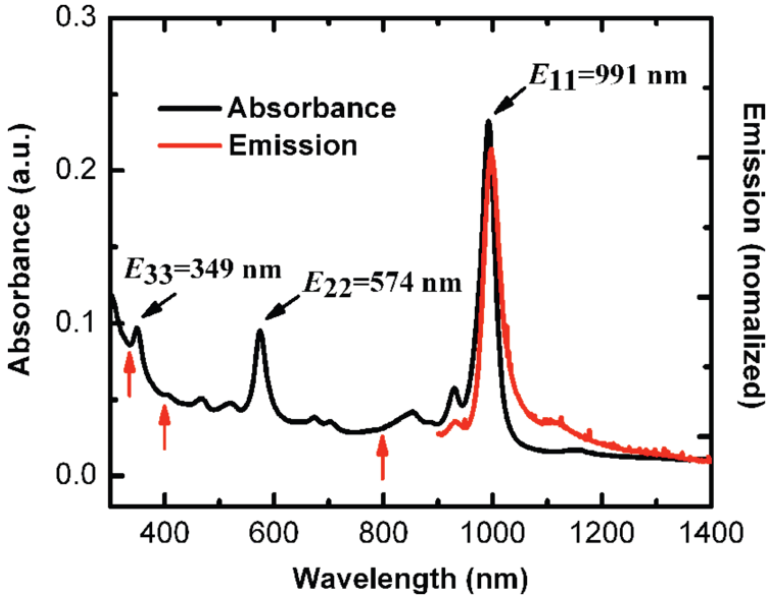

FIGURE 1. Absorption and fluorescence spectra of the DNA-wrapped
(6, 5) enriched SWNT sample. The first, second, and third excited
excitonic states are labeled in the figure. The vertical red

The experimentals for SWNT as a quantum dot

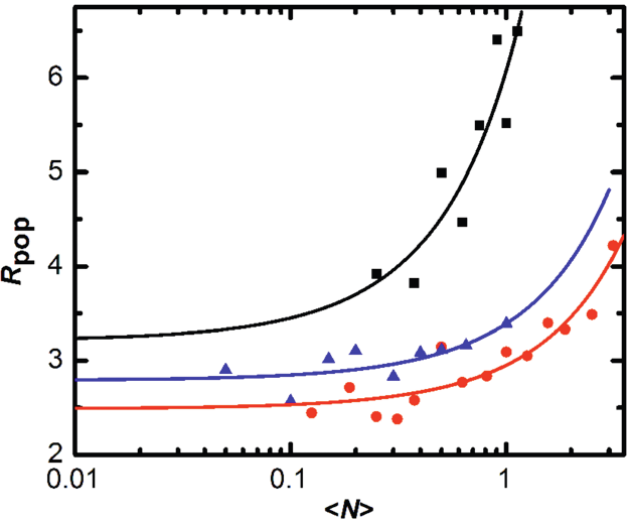

Ratio of exciton population at tE) 0.2 ps and tL) 13 ps (Rpop) with excitation at 800 nm (red circles), 400 nm (blue triangles), and 335 nm (black squares).（Ref. Multiple Exciton Generation in Single-Walled Carbon Nanotubes）

In 2010, Todd D. Krauss measured the absorption and fluorescence spectra of the DNA-wrapped (6, 5) enriched SWNT sample.using ultrafast transient absorption spectroscopy, he has measured MEG processes in (6,5) SWNT and found a QY of 130% under 335 nm excitation and 110% under 400 nm excitation. These results suggest that the MEG threshold in SWNTs can be close to the thermodynamic limit of 2Eg. Overall, the observation of MEG process and faster Auger recombination in SWNTs relative to Nano Ctystals is in agreement with the physical picture that electrons and holes in SWNTs experience stronger confinement and have enhanced many-body effects when compared to Nano Crystals.(Ref.Multiple Exciton Generation in Single-Walled Carbon Nanotubes)

In 2012, Satoru Konabe and Susumu Okada investigated theoritically that multiple excitons can be directly generated by a single photon through resonant coupling with multiexciton states. Further, the theoretically predicted threshold energy for this process is consistent with recent experimental results. Our calculations clarify the elementary processes of multiple-exciton generation in single-walled carbon nanotubes

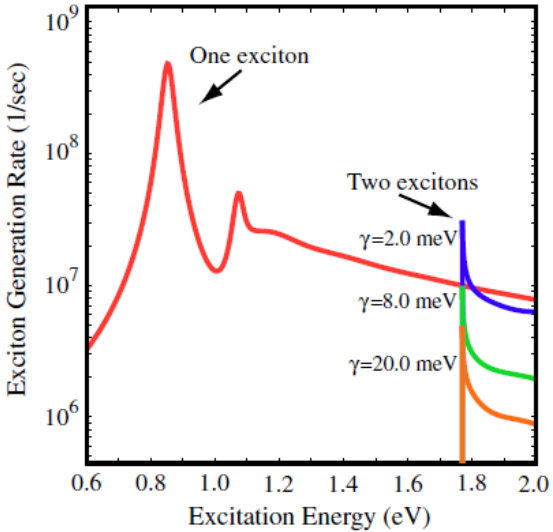

Generation rates for one and two excitons by a single photon.(Ref. Multiple Exciton Generation by a Single Photon in Single-Walled Carbon Nanotubes)

Proposed MEG mechanism of Single wall carbon nanotube

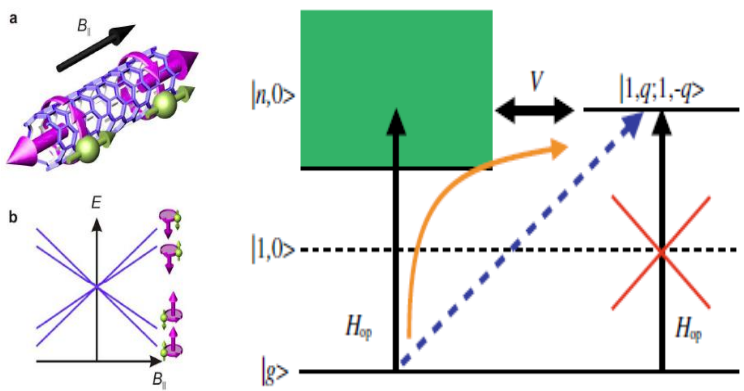

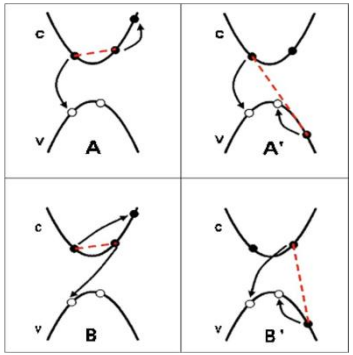

$$\Gamma_{MEG}(\omega) = \frac{2\pi}{\hbar}\sum_{q}\left|\sum_{n}\frac{\langle g|\mathcal{H}_{op}|n,0\rangle\langle n,0|V|1,q;1,-q\rangle}{E_q^1 + E_{-q}^1 - E_0^n + i\gamma}\right|^2 \times \delta(\hbar\omega - E_q^1 - E_{-q}^1$$

$$\Gamma_{Auger} = \frac{A}{L}\cdot N(N-1) \approx= 128\frac{\omega_{vc}}{k_{e0}}\cdot\left(\frac{\mu}{m_0}\right)\left(\frac{E_b}{E_g}\right)^3\cdot L\cdot n^2$$

The difference between nanocrystals and SWNTS

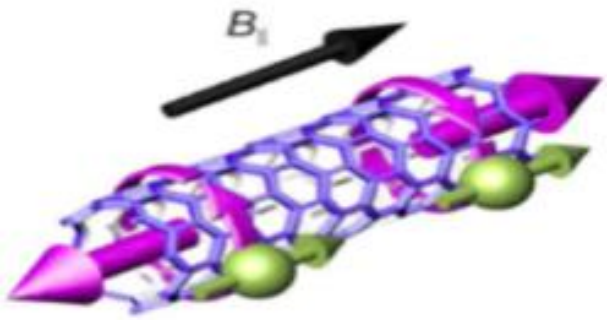

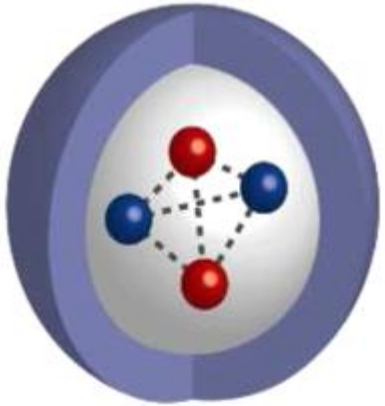

One of the most important difference between nanocrystals and SWNTs is the conservation restriction applying for the MEG process. The MEG of nanocrystals obeys only energy conservation, while the MEG of SWNTs obeys the energy conservation, momentum conservation, and the angular momentum conservation

The basic reason for SWNT as quantum dot

1 Two dimensional quantum confinement of electrons and holes around the SWNT circumference leads to a distinctive density of states and well-defined selection rules for discrete optically allowed transitions.(Ref. Carbon Nanotubes, Advanced Topics in the Synthesis, tructure, Properties and Applications; Jorio, A., Dresselhaus, G., Dresselhaus, M. S., Eds.; Topics in Applied Physics, Vol. 111; Springer:Berlin and New York, 2008; pp 1-720)

2 Like semiconductor Nano Crystals, SWNTs exhibit a strong Coloumb interaction between electons and holes(Ref. Spataru, C. D.; Ismail-Beigi, S.; Benedict, L. X.; Louie, S. G. Phys.Rev. Lett. 2004, 92, 077402.Perebeinos, V.; Tersoff, J.; Avouris, Ph. Phys. Rev. Lett. 2004, 92,257402.;Huang, L. B.; Krauss, T. D. Phys. Rev. Lett. 2006, 96, 057407.)

3 SWNTs can be used to systematically analyze the fundamental mechanism of MEG since their sizes and structures have been well

2 Challenge of MEG of SWNT quantun dot

Three steps are required for generation of electrical power:
i)absorption of photons from the sun;
ii) photoinduced charge separation and the generation of mobile carriers;
iii) collection of electrons and holes at opposite electrodes

Challenges: Coexist of Multiple Exciton Generation and Recombination of excitons caused by Auger process

1 the competition between MEG and Auger recombination;

2 interface morphlogy for electron transfer

3 The competition between MEG and Auger recombination result in low carrier efficiency

3 Challenge of MEG of SWNT quantun dot

- Competition of multiple exciton generation and Auger recombination of single wall carbon nanotube investigated by The perturbation theory

MEG and Auger Recombination within Bulk crystals and nano crystals

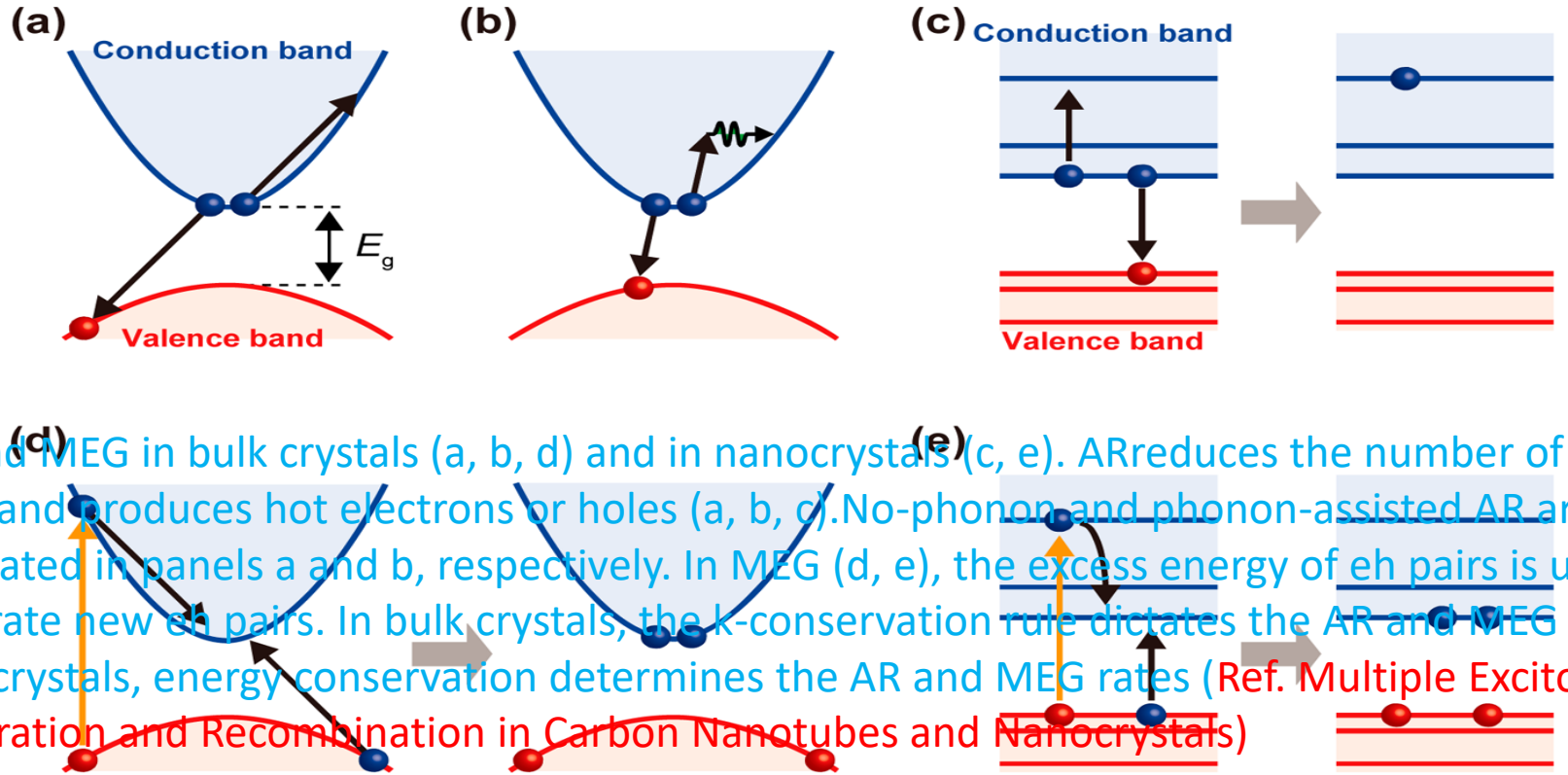

AR and MEG in bulk crystals (a, b, d) and in nanocrystals (c, e). ARreduces the number of eh pairs and produces hot electrons or holes (a, b, d).No-phonon and phonon-assisted AR are illustrated in panels a and b, respectively. In MEG (d, e), the excess energy of eh pairs is used to generate new eh pairs. In bulk crystals, the k-conservation rule dictates the AR and MEG rates. In nanocrystals, energy conservation determines the AR and MEG rates (Ref. Multiple Exciton Generation and Recombination in Carbon Nanotubes and Nanocrystals)

Multiple Exciton Generation by a Single Photon in Single-Walled Carbon Nanotubes

The perturbation theory has successfully explained, for instance, the Augerrecombination rate of excitons in SWNTs。After utilizing the first order perturbation regarding the Coulomb interaction V,he ground state becomes

- $|\tilde{g}\rangle = |g\rangle + \sum_{\mu} |\mu\rangle \frac{\langle \mu|V|g\rangle}{E_0 - E_\mu} + \sum_{\mu,v} |\mu; v\rangle \frac{\langle \mu; v|V|g\rangle}{E_0 - E_{\mu,v}}$ (1)
- the two-exciton state, becomes：
- $|\widetilde{\mu; v}\rangle = |\mu; v\rangle + \sum_{\mu'} |\mu'\rangle \frac{\langle \mu'|V|\mu; v\rangle}{E_{\mu,v} - E_{\mu'}} \times \sum_{\mu',v' \neq \mu,v} |\mu'; v'\rangle \frac{\langle \mu'; v'|V|\mu; v\rangle}{E_{\mu,v} - E_{\mu',v'}}$ (2)

The direct generation of two excitons by a single photon is forbidden by the selection rule, as shown in Fig. 1. Using the perturbed states (1) and (2),, the MEG rates are calculated by the following expression of the Fermi goldenrule

$$\Gamma_{MEG}(\omega) = \frac{2\pi}{\hbar}\sum_q \left|\sum_n \frac{\langle g|\mathcal{H}_{op}|n,0\rangle\langle n,0|V|1,q;1,-q\rangle}{E_q^1+E_{-q}^1-E_0^n+i\gamma}\right|^2 \times \delta\left(\hbar\omega - E_q^1 - E_{-q}^1\right) \quad (3)$$

MEG can occur at an excitation energythat satisfies the relation, which is representedby the Dirac delta function. We phenomenologically consider the dephasing processes for the intermediate states by accounting for the dephasing rate _x0004_ in the denominatorof Eq. (3).The exciton amplitude Zn k;q and energy Enq are obtained by solving the Bethe-Salpeter equation

$$\left(\varepsilon^{c}_{k+q} - \varepsilon^{v}_{k}\right)Z^{n}_{k,q} + \sum_{k'} K_{k,k'} Z^{n}_{k',q} = E^{n}_{q} Z^{n}_{k,q} \qquad (4)$$

the conversion rates for one and two exciton generation.

The one-exciton generation rate is given by

$$\Gamma_{s}(\omega) = \frac{2\pi}{\hbar}\sum_{n} \left|\langle n, 0 | \mathcal{H}_{op} | g \rangle\right|^{2} \delta(\hbar\omega - E^{n}_{0}) \qquad (5)$$

On the other hand, rapid exciton-exciton annihilation through an auger recombination enhance as the density of exciton increase, The Auger recombination rate is calculated by

$$\Gamma_{Auger} = \frac{A}{L} \cdot N(N-1) \approx= 128 \frac{\omega_{vc}}{k_{e0}} \cdot \left(\frac{\mu}{m_0}\right) \left(\frac{E_b}{E_g}\right)^3 \cdot L \cdot n^2$$

(7)

E_b, The strength of binding energy， E_g the energy gap between conduction and convalence

The rate of Auger recombination is intimate with the The strength

3 Our solution to Quantum dot solar cells: Heterojuncture of Conjugated polymer/carbon nanotube

Heteroconjunction, a complex of Multiple Exciton Generation of Quantun dot in heterogeneous π complexes of conjugated polymer and carbon nanotube was proposed

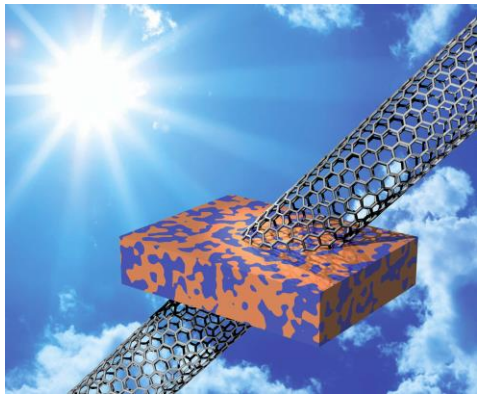

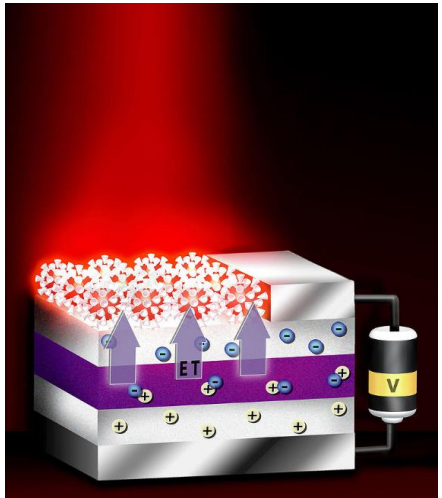

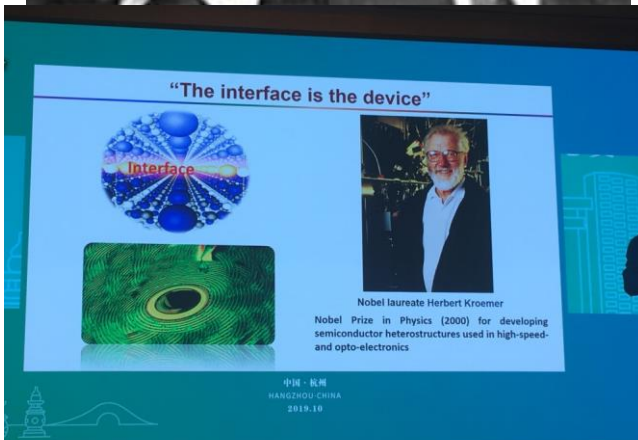

3 Our solution to Quantum dot solar cells: Heterojuncture of Conjugated polymer/carbon nanotube Bulk Heterojunction of Conjugated Polymer

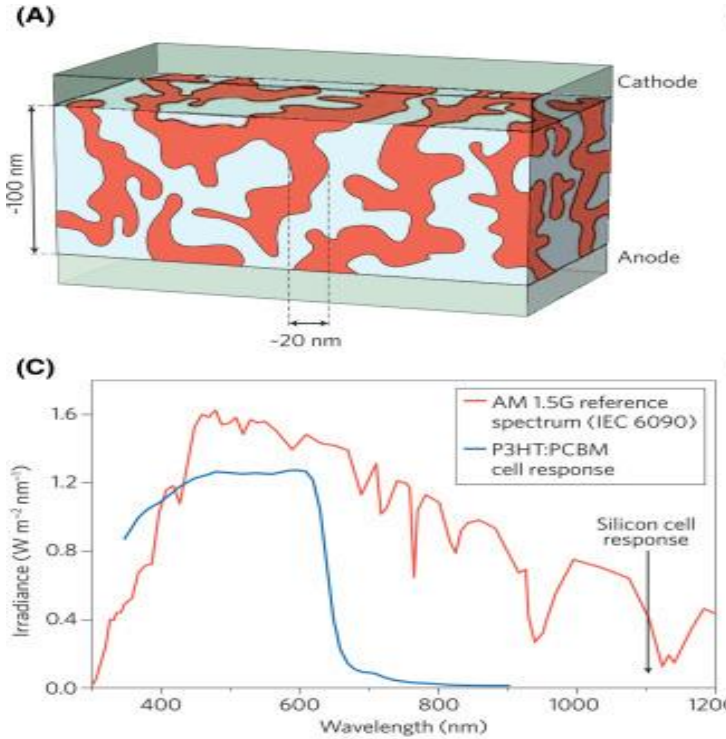

3 Solution to ultrafast electron transver **Bulk heterojunction solar cells**

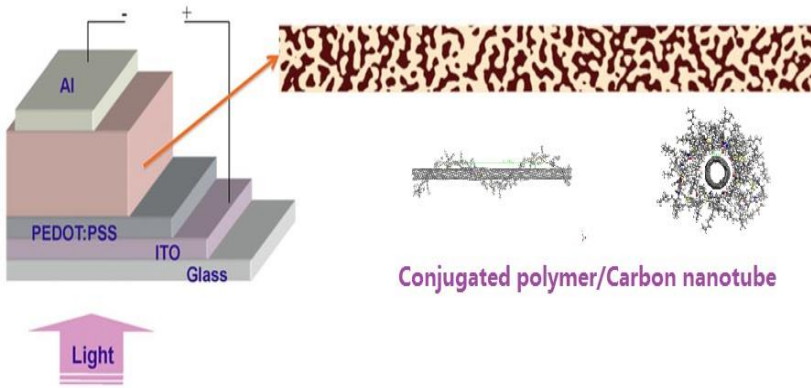

The Phase separated BHJ Morphology is critical to charge collection

Self-assembly is required to achieve the phase-separated nano-morphology at the 10–20 nm length scale.

Phase separation and connected pathways are required to achieve suffi ciently high carrier mobility to enable the charge to reach the electrodes prior to recombination.

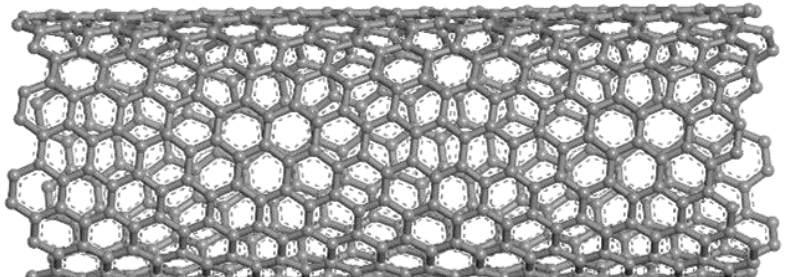

3.1 Our solution, Experimental Results

IN 2018 we choose the conjugated polymer PIDT-BT with a band gap *E*g≈ 1.71 eV; SWCNTs (obtained from Sigma-Aldrich with the following parameters: 98% semiconducting, 2% metallic, with the length ca. 0.3–5 μm, diameter of ca. 1.2–1.7 nm, a density of ca. 1.7–1.9 g/cm3) and used without additional treatment

(a)

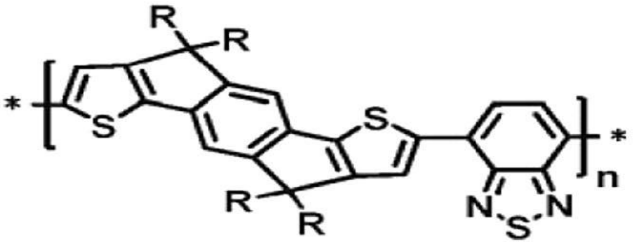

R = 4-*n*-hexylphenyl

(b)

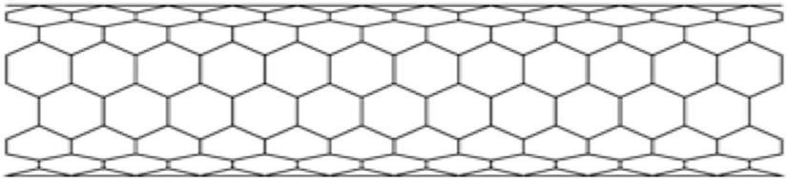

Materials and preparation

Both components were dissolved and dispersed separately in chloroform. Subsequently, the solutions were mixed with relative amounts of 1:0.1 and 1:0.3 and subjected to ultrasonic treatment for 10 min on a Bandeline Sonopuls HD 2070 ultrasonic mixer (at a frequency $f \approx 20$ kHz). The resulting solution was applied by drop-cast technique at a temperature of 300 K in an atmosphere of N_2 on glass substrates with thermally evaporated gold (Au) electrodes on top.

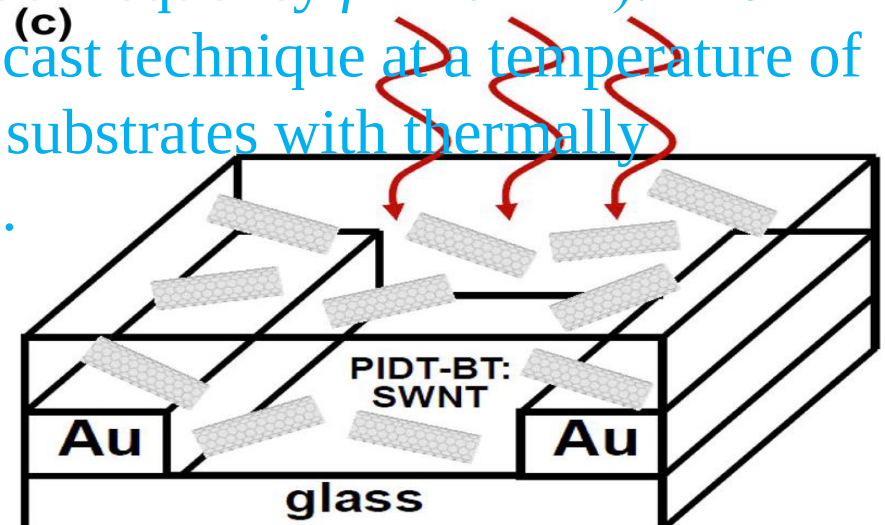

We used the usual lithography technique to obtain an electrode spacing of ≈ 15 μm.) Afterward, the films were dried at 100 ° C under N_2 for 10 min and kept in vacuum desiccator (MB SANPLATEC Corp.) until measurements. Thus, in our study, we are dealing with films with hole-only conductivity based on PIDT-BT, with weakly and intermediate doped with SWCNT, which are referred to as composite films in the text. The morphology of the PIDT-BT/SWCNT composite films was investigated by atomic force microscope (AFM)—Solver P47-NT-MDT. The thickness of the films obtained by drop casting onto quartz substrates was ≈ 1 μm, according to the AFM data.

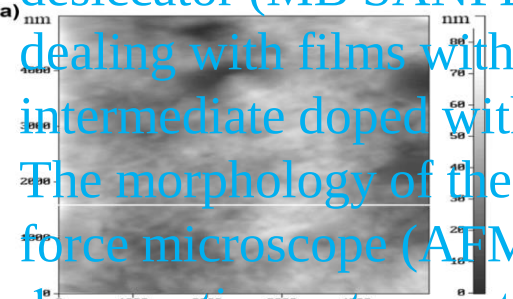

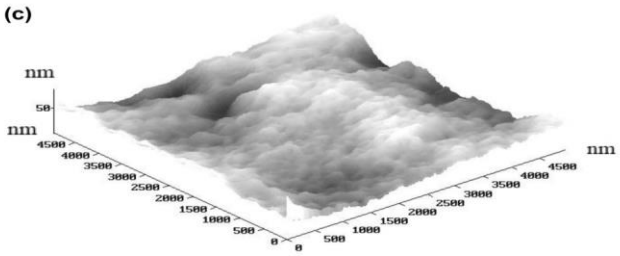

AFM

The results of AFM investigations of the PIDT-BT/SWCNT (1:0.3) film are shown in Fig. 2a–c. As can be seen from these figures, the surface of PIDT-BT/SWCNT nanocomposite films was moderately rough. We found that the overall height variation was about 50–100 nm, exhibiting steps of several nm (Fig. 2b), which may reflect SWCNTs and their agglomerates covered with the PIDT-BT polymer. It was found that the average roughness and root-mean-square (RMS) values of the PIDT-BT/SWCNT film (1:0.3) as shown in Fig. 2a–c are about 8.8 nm and 11 nm, respectively. Theseparameters are higher than that of a pure PIDT-BT film, where the average roughness and root mean square are 4 nm and 5 nm, respectively (not shown). As can be seenfrom our AFM measurements, the modification of the PIDTBT polymer with SWCNT led to a relatively smooth surface of the PIDT-BT/SWCNT composite films

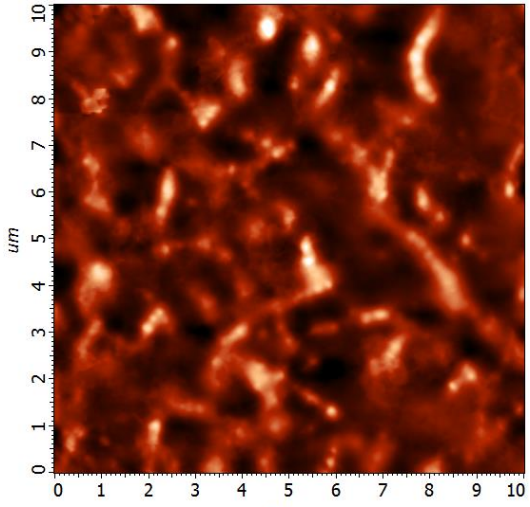

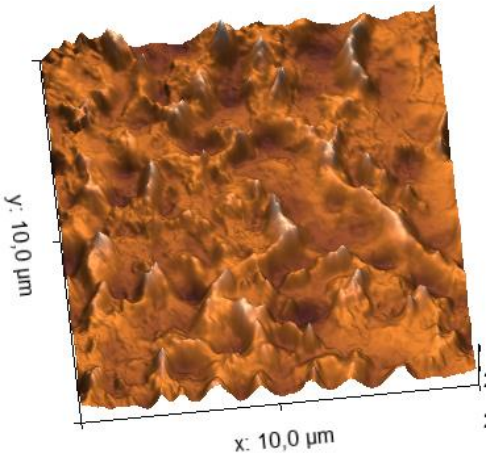

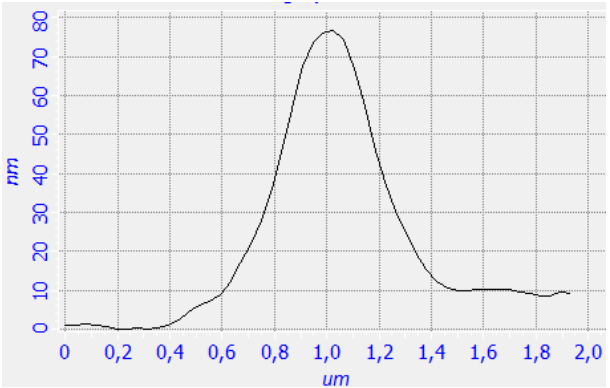

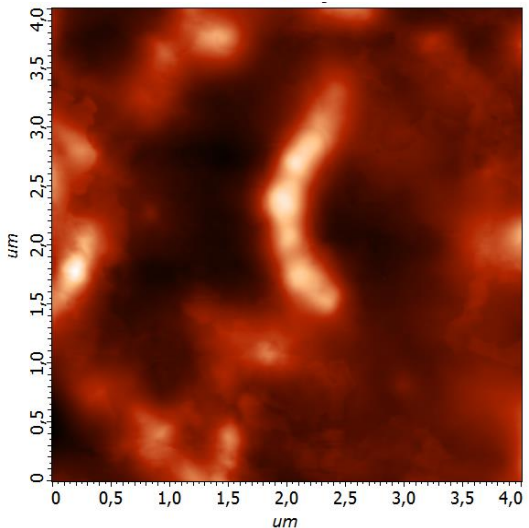

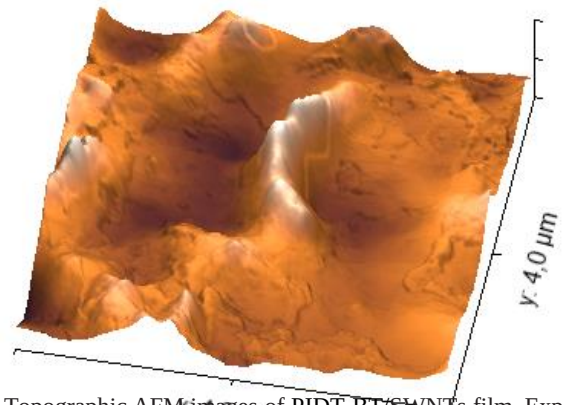

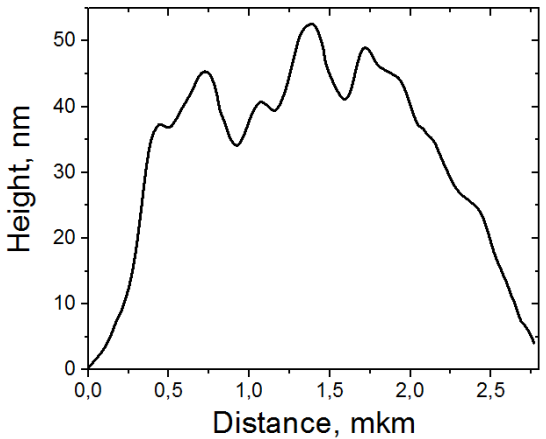

(a) Topographic AFM images of PIDT-BT/SWNTs film. Experimental conditions: sonication time 20 min; Si surface; tapping mode; (c) PIDT-BT/SWNT height profile histogram of the panel a data: perpendicular and parallel to the SWNT directions. (c) Height profile along the SWNT in panel c) showing the periodic height oscillation that derives from PIDT-BT helical wrapping of the SWNT.

Absorbance spectra of pure PIDT-BT (1) and PIDT-BT/SWCNT (1:0.3) (2) films

Figure 3 shows typical absorbance spectra of neat PIDTBT (1) and PIDT-BT/SWCNT (1:0.3) films (2) deposited onto quartz substrates. As can be seen from Fig. 3, the absorbance spectra of PIDT-BT and PIDT-BT/SWCNT (1:0.3) films were in the spectral region from 200 nm to 800 nm. It was found that the absorbance onset for PIDT-BT and PIDT-BT/SWCNT (1:0.3) films is abo correlates well with the band gap of th evident from Fig. 3, adding of about 3(matrix resulted in a decrease in absorb absorbance maxima (at ~ 688 nm and

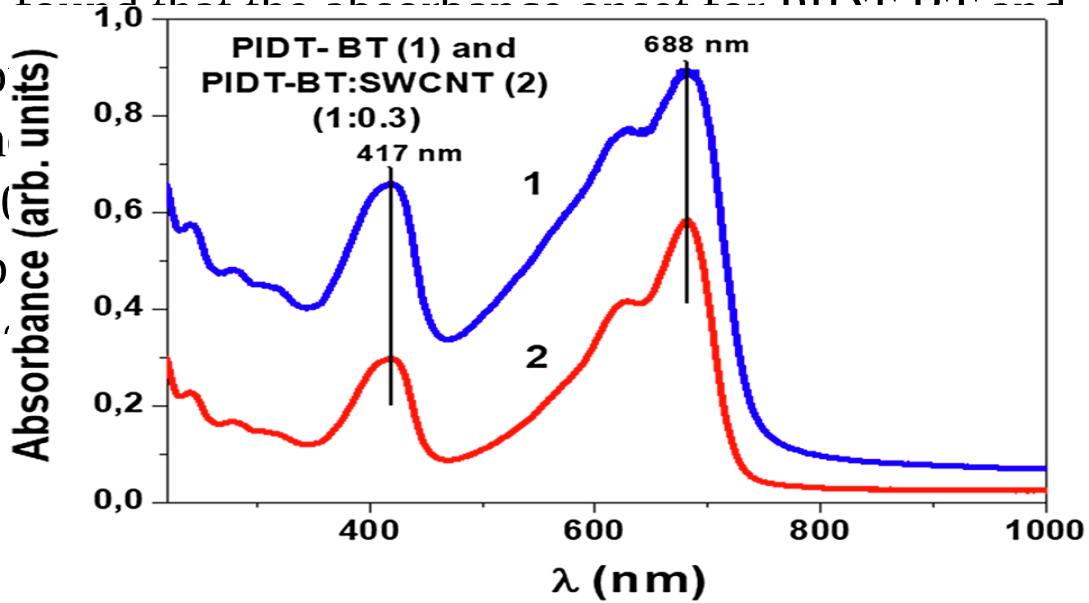

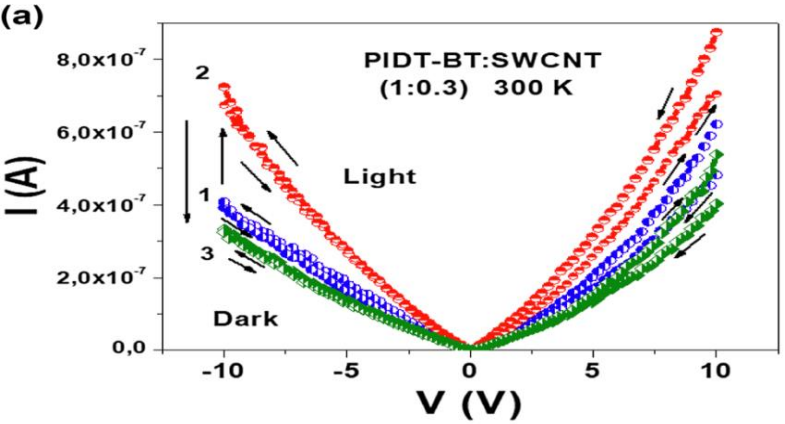

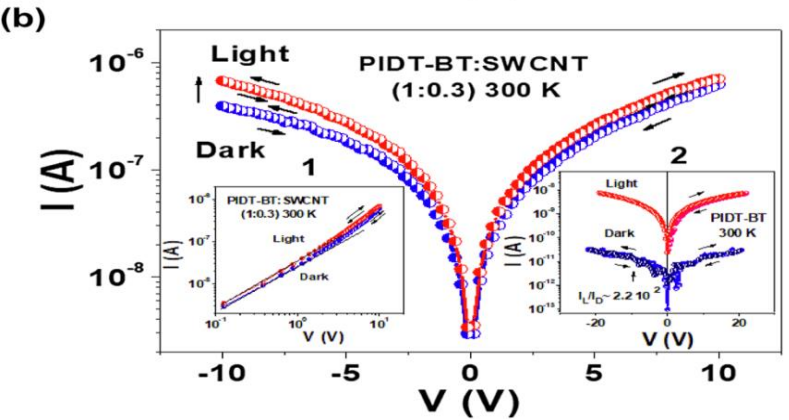

the DC conductivity of the neat PIDT-BT polymer film was lower by two orders of magnitude compared with PIDTBT/SWCNT (1:0.3) film; The dark current of pure PIDT-BT is very low, but it increases by two orders of magnitude after illumination with a solar simulator

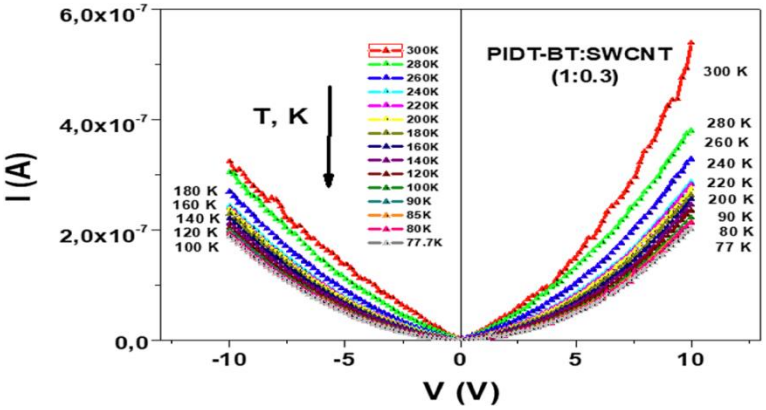

I–Vs of the PIDT-BT/SWCNT (1:0.3) nanocomposite film measured in the dark at different temperatures within the temperature interval from 300 to 77 K at T[K] =300, 280, 260, 240, 220, 200, 180, 160, 140, 120, 100, 90, 85, 80, 77

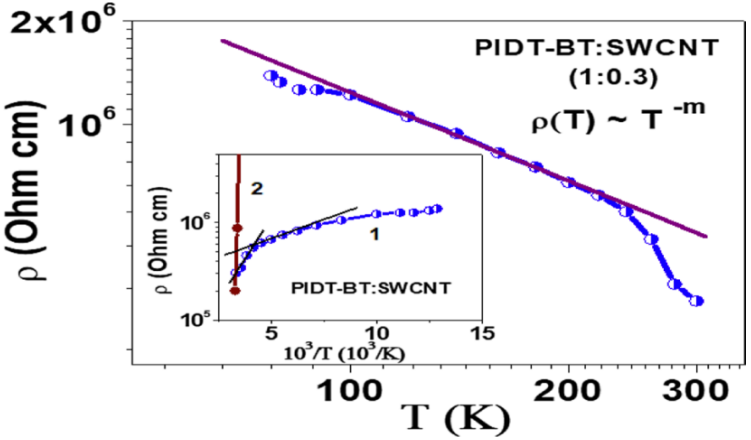

Temperature dependence of the resistivity of the PIDT-BT/ SWCNT (1:0.3) nanocomposite film. Inset: ρ(T) vs. 103/ T dependences
for the same PIDT-BT/SWCNT (1:0.3) sample (curve 1) and for PIDT-BT/SWCNT (1:0.1) (curve 2) nanocomposite film

I–Vs demonstrated an increase in photocurrent under illumination at 300 K by factor of ca. 1.4–1.7 with respect to dark *I–Vs*.

3.2 Our solution, Theoritical Results

- Conjugated polymer with prefered geometry and semi-conductor carbon nanotube and metal carbon nanotube

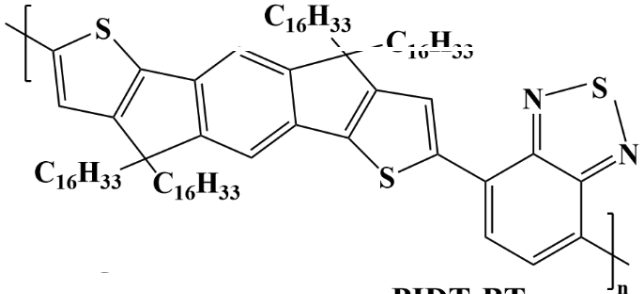

PIDT-BT

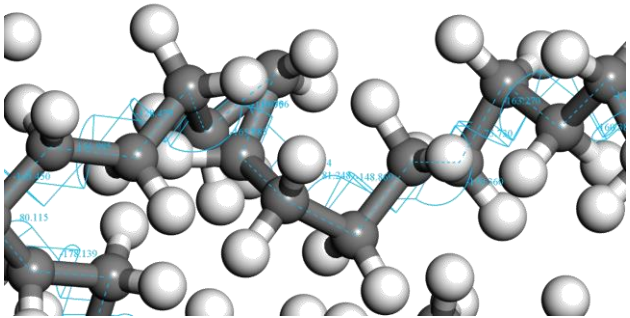

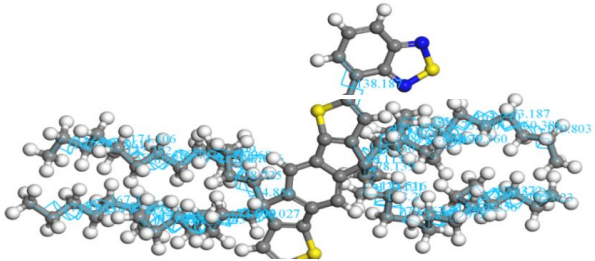

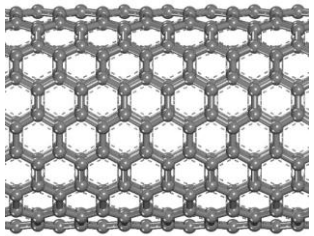

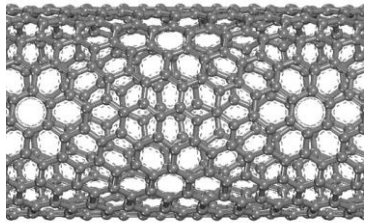

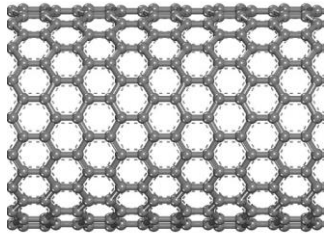

（a）SWCNT（9,9）　（b）SWCNT（12,8）　（c）SWCNT（18,0）

Preferred conformation of conjugated polymer wrapping around SWNT

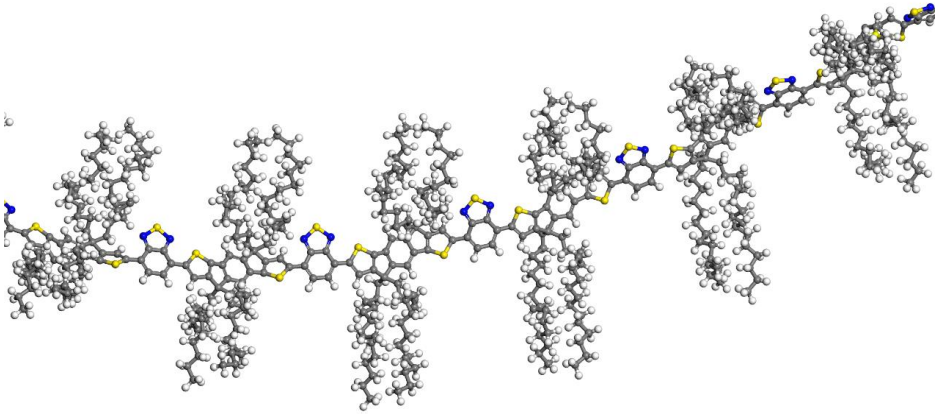

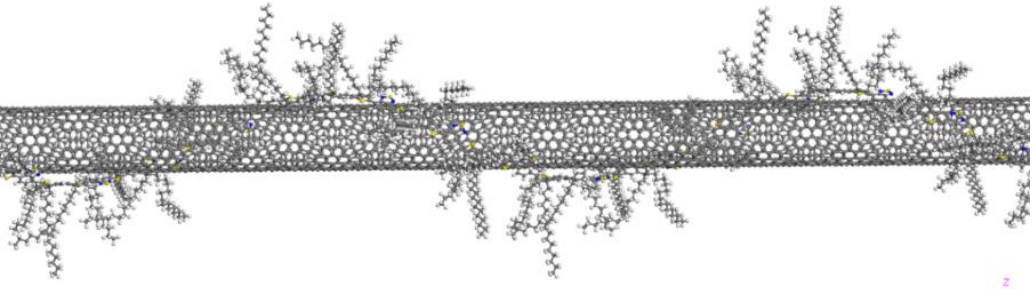

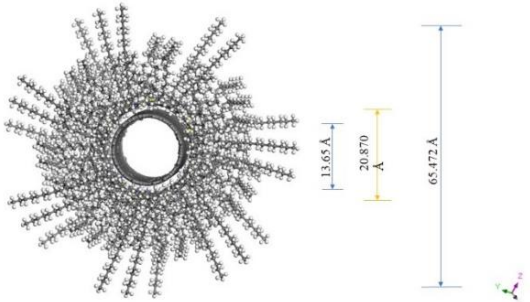

Helix conformation of conjugated polymer winding carbon nanotubes

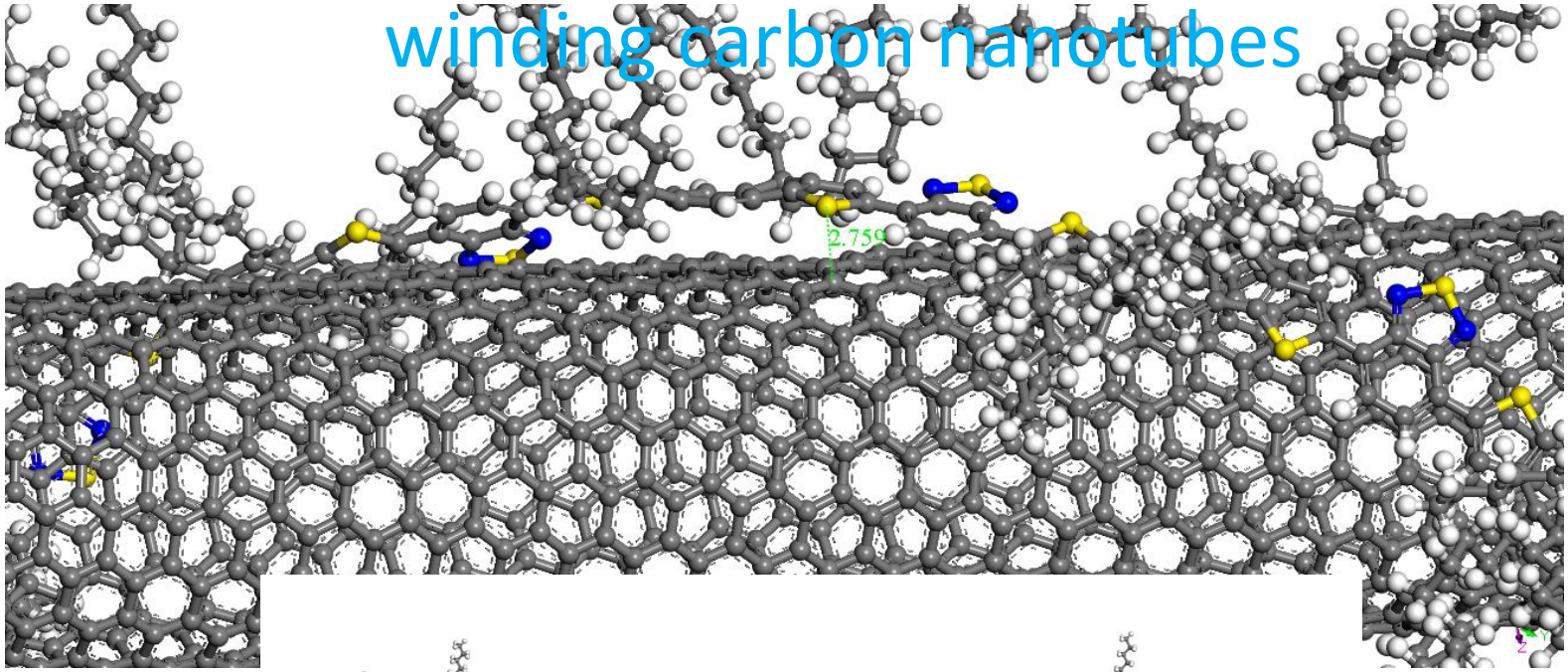

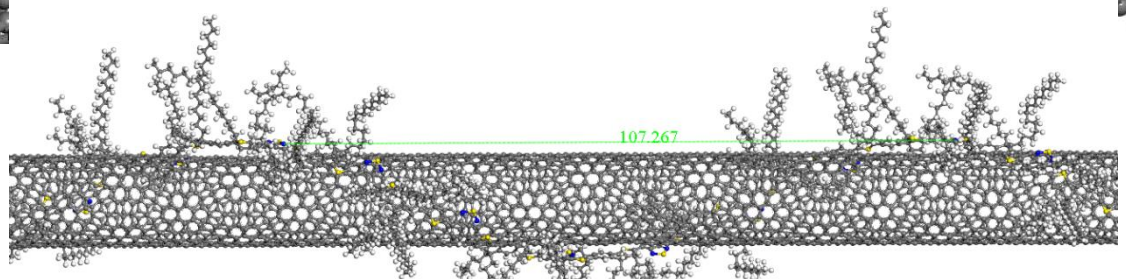

Helix conformation of conjugated polymer winding carbon nanotubes

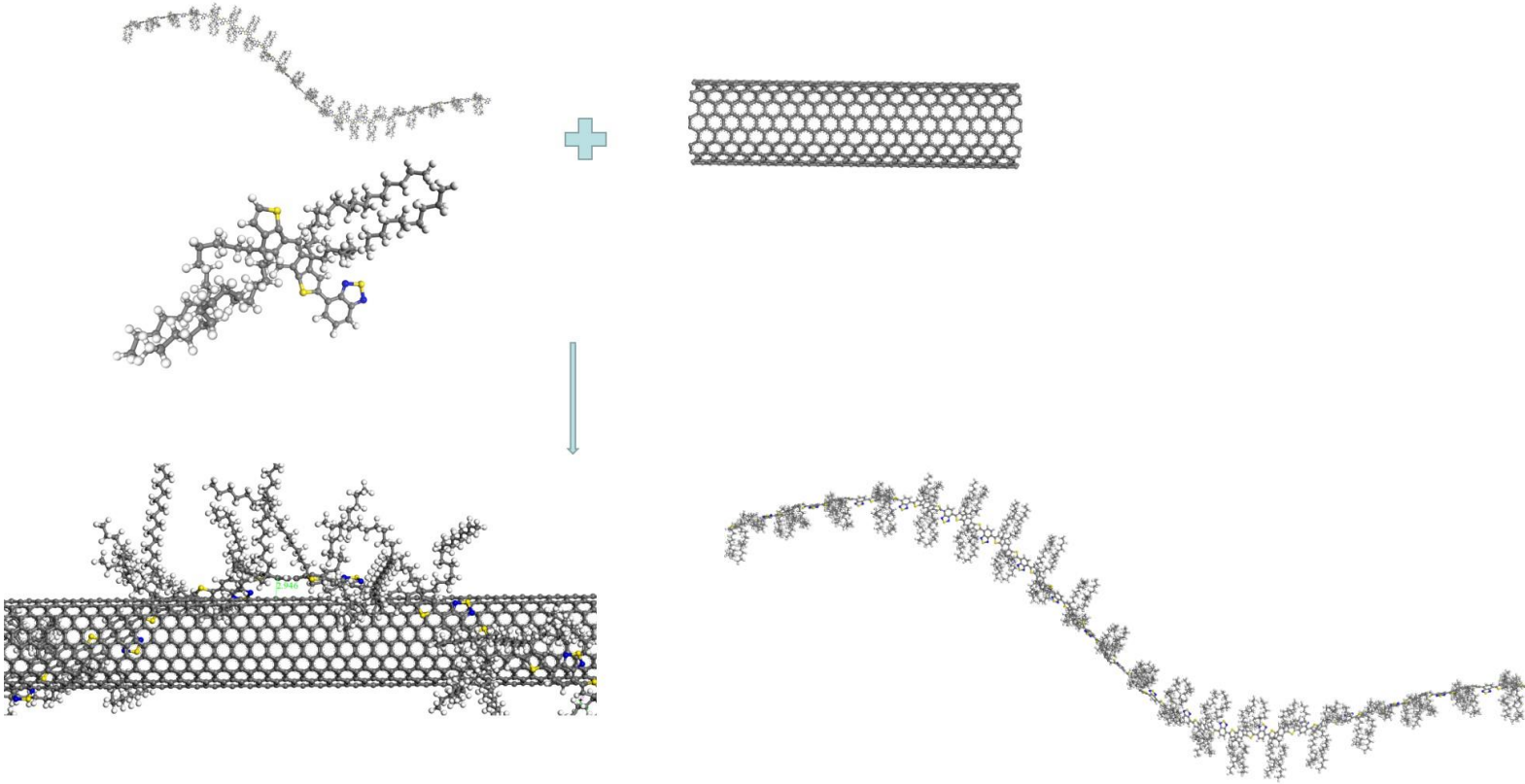

Constructing model of PIDT-BT and single wall carbon nanotube

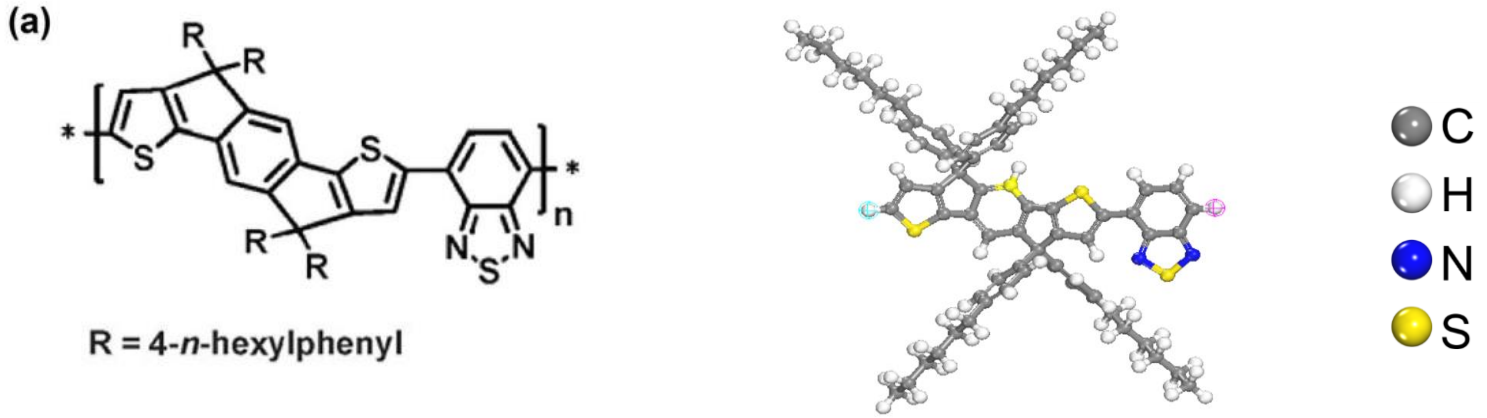

左图为PIDT-BT分子式，右图为PIDT-BT单体，下图为聚合度为10的PIDT-BT共轭聚合物分子链构型

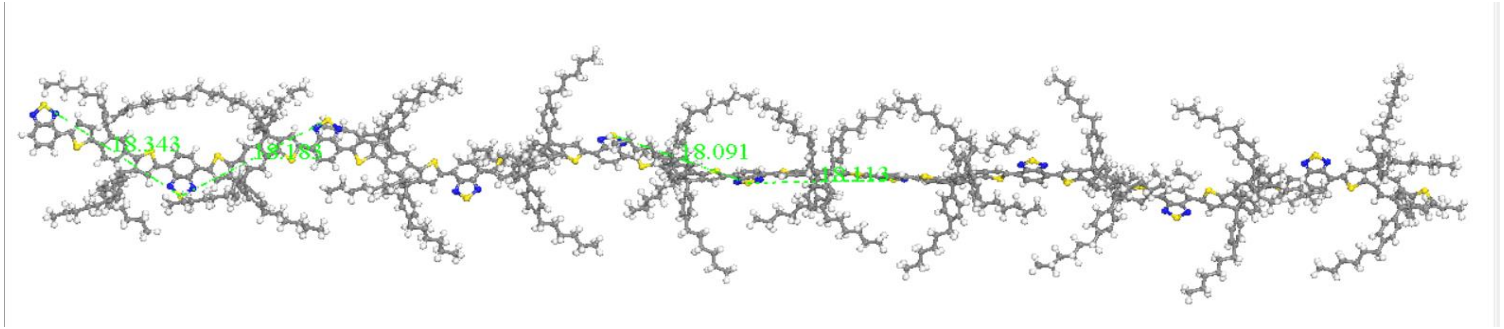

Interaction between PIDT-BT and (9,9)SWCNTs and preferred winding confomation of Conjugated polymer PIDT-BT

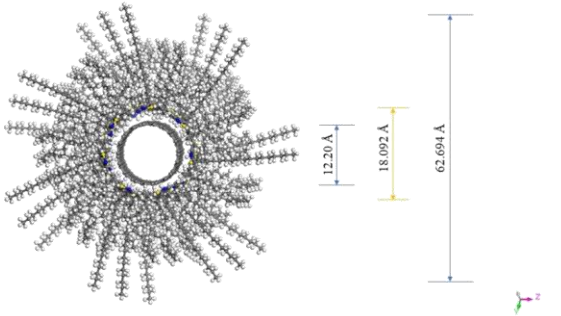

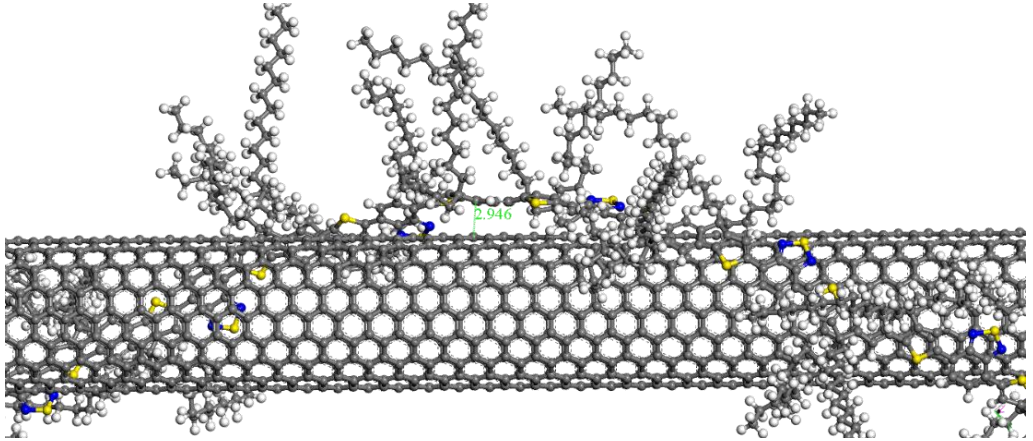

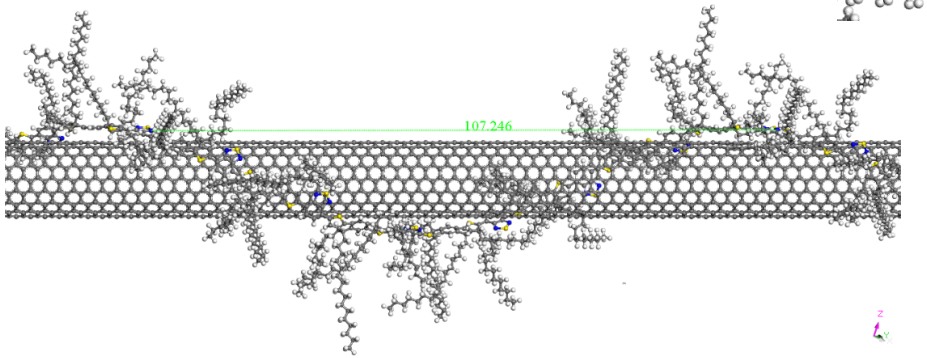

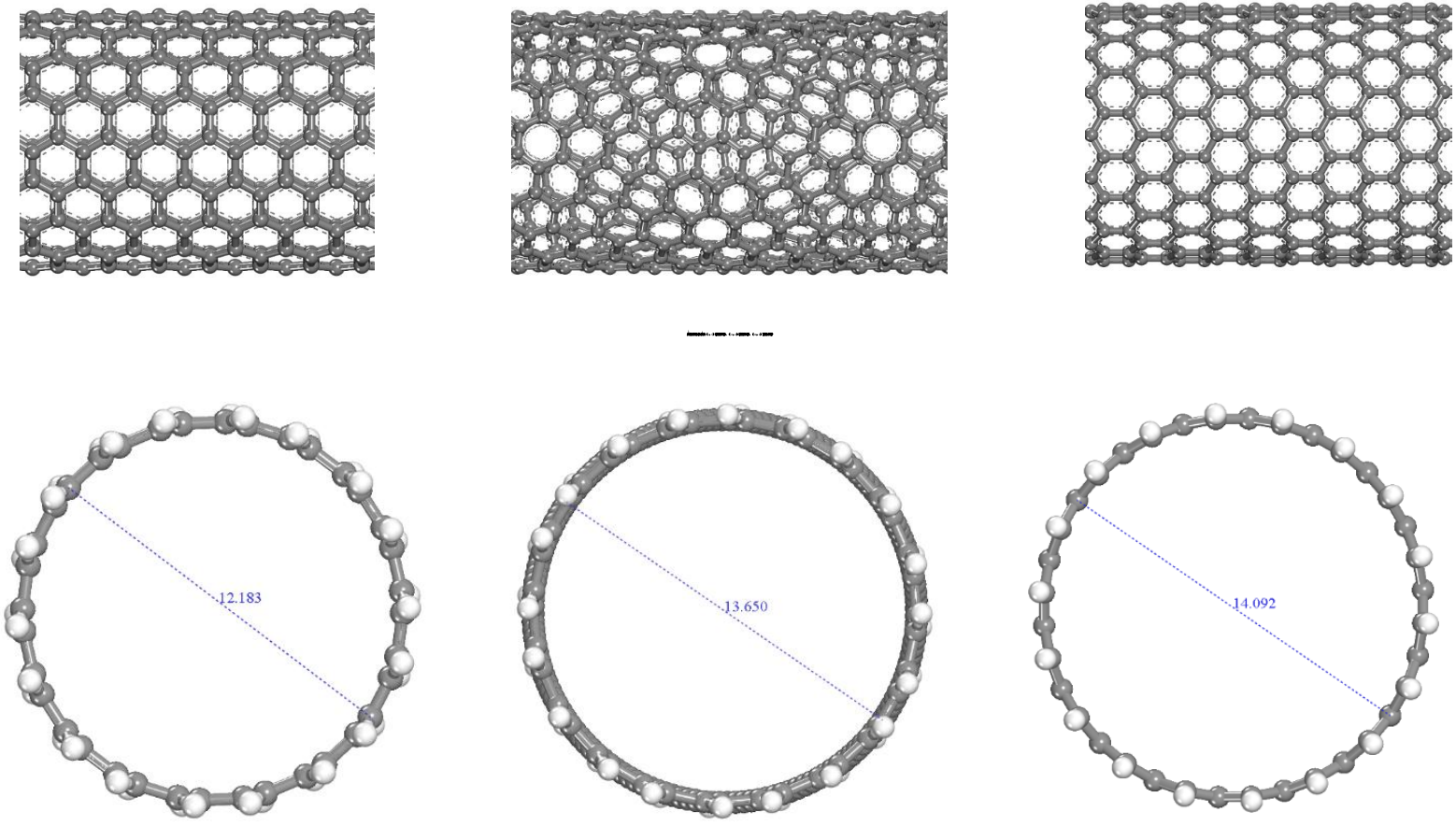

（a）SWCNT（9,9）　（b）SWCNT（12,8）　（c）SWCNT（18,0）

PIDT-BT/SWCNTs（9，9）Molecular dynamics of preferred conformation of PIDT wrapping CNT and and DFT simulation of CDensity of State

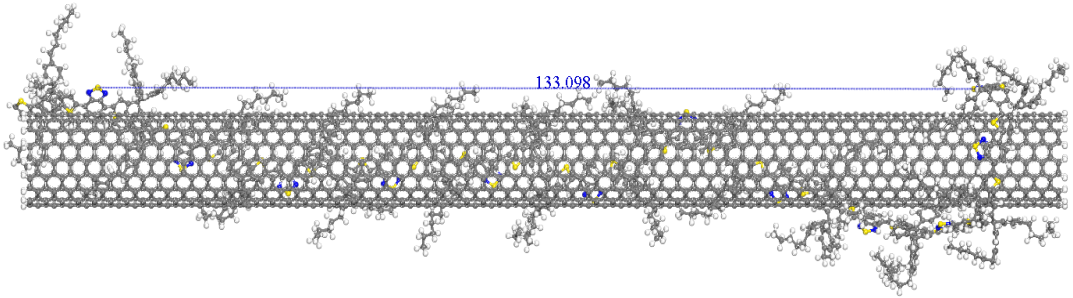

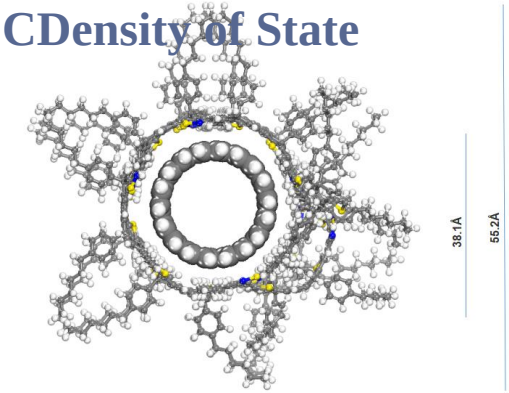

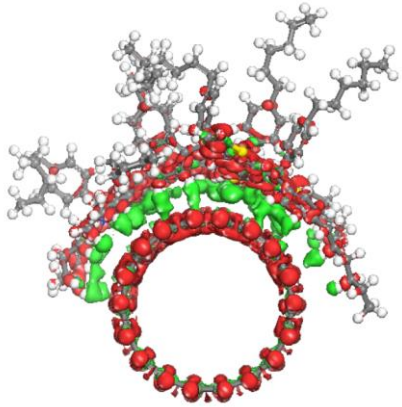

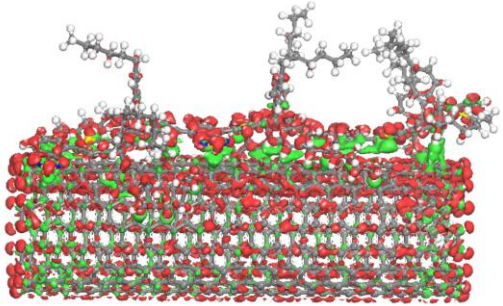

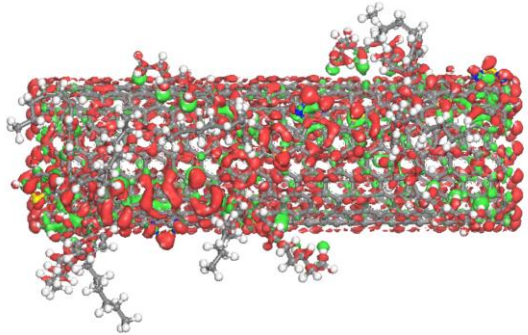

PIDT-BT/SWCNTs（12，8）Molecular dynamics of preferred conformation of PIDT wrapping CNT and and DFT simulation of

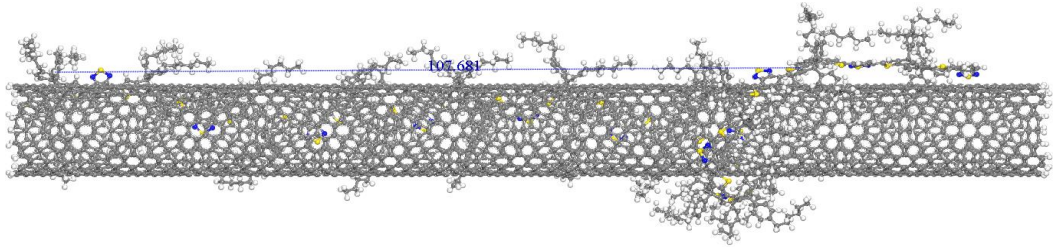

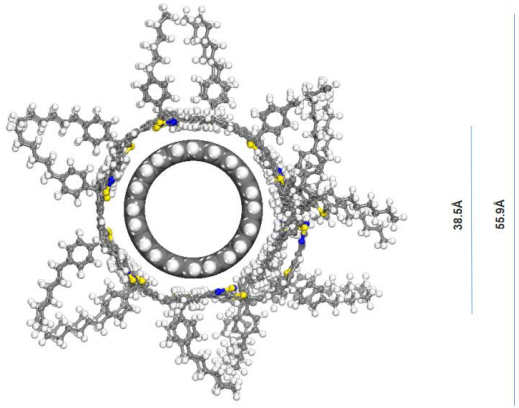

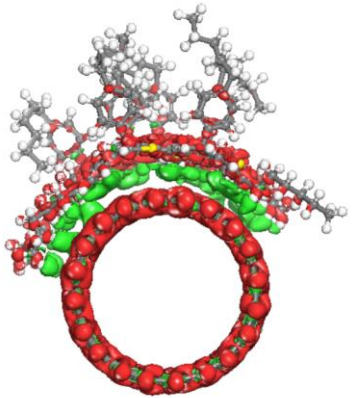

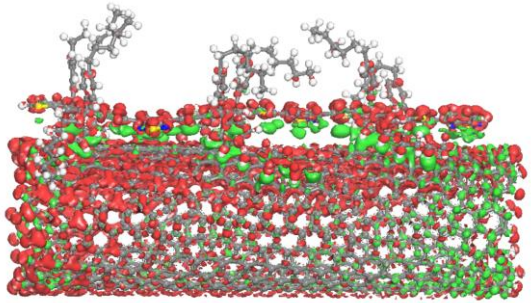

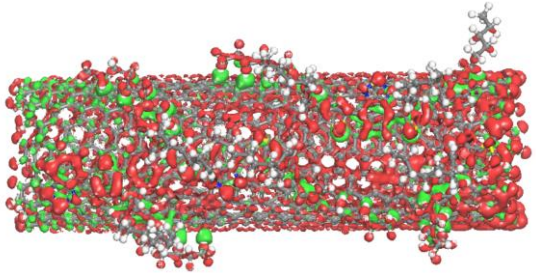

PIDT-BT/SWCNTs（18，0）Molecular dynamics of preferred conformation of PIDT wrapping CNT and and DFT simulation of CDensity of State

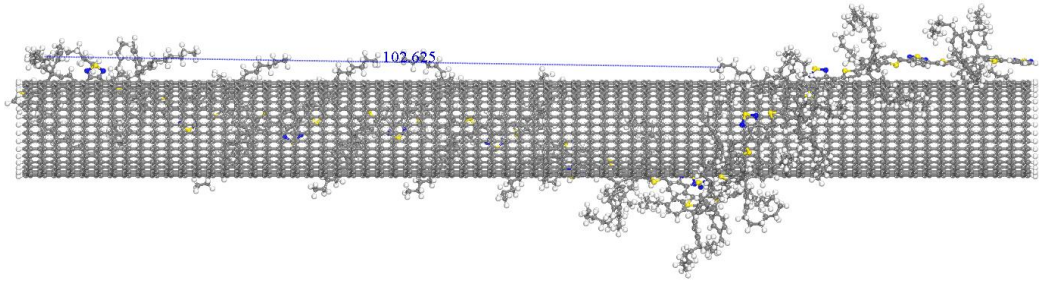

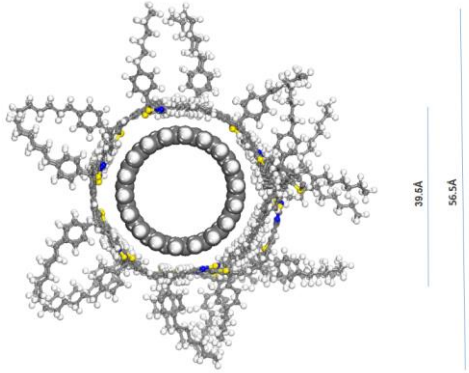

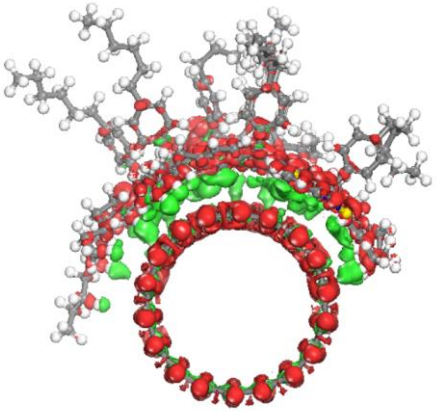

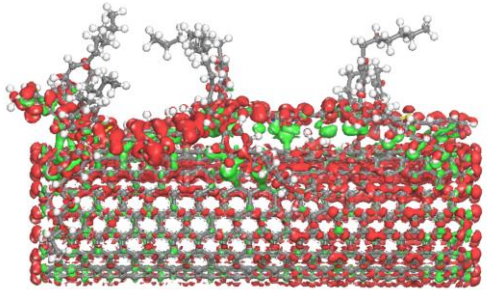

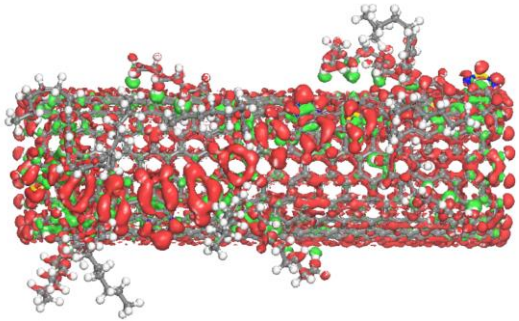

Table 1 Comparison of preferred winding confomation of Conjugated polymer PIDT-BT around three types single wall carbon nanotube

	（9，9）SWCNTs	(12,8)SWCNTs	(18，0)SWCNTs
Pitch (conjugated polymer winding around CNT)/Å	107.246	107.267	107.226
Interfacial distance/Å	2.946	2.759	2.584
Diameter of CNT/Å	12.20	13.65	14.09
Average temperature/K	419.259	288.667	335.841
Average total energy/(kcal/mol)	10252.640	14859.357	10642.702
Average potential/(kcal/mol)	8595.497	13611.688	9279.236
Average kinetic energy/(kcal/mol)	1657.144	1247.668	1363.466
Non convalent energy/(kcal/mol)	88.486	-59.187	-53.609

Charge separation at PIDT-BT/CNT interface is the key determinableo charge generation efficiency for PV applications, which depends significantly on the interfacial energy band alignment between the donor and acceptor species, and the donor–acceptor coupling.The information can be obtained from the density of states (DOS). The DOSs of PIDT - BT(black line) and three types of (9,9) (12,8)(18,0)CNT (red line), respectively, which indicates that PIDT-BT interfaced with (9,9) (12,8)(18,0) CNT is formation of type-II PV heterojunctions.

Density of state of complex of three CNT and conjugated polymer

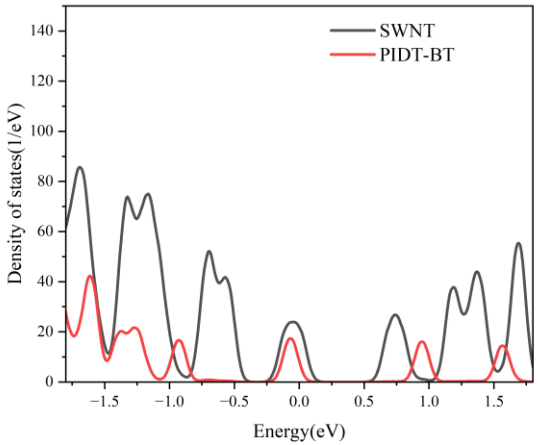

DOS of PIDT-BT/SWCNT（9，9）

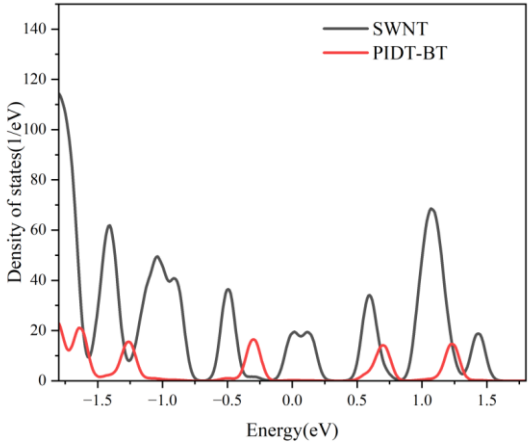

DOS of PIDT-BT/SWCNT（12，8）

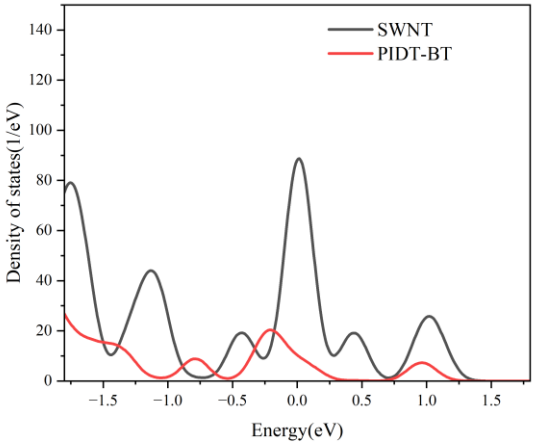

DOS of PIDT-BT/SWCNT（18，0）

Figure The density of States (DOS) (a) PIDT-BT/CNT (9,9) interface, (b) PIDT-BT/CNT (12,8) interface and (c) PIDT-BT/CNT (18,0) . The DOS of PIDT-BT and CNT species are plotted in black and red lines, respectively. The Fermi level is set to zero. DOS shows formation of type-II heterojunction between P3HT and (9,9) (12,8)(18,0) CNT , respectively

This resonance is ascribed to the unique characteristics of SWNTs that originate from their quasi one dimensional structures, resulting in a strong Coulomb interaction between excitons competing with phonon dephasing and the van Hove singularity in the density of states of the two-exciton states.

Discussion of DFT

The HOMO of the PIDT-BT/(9,9) (12,8)(18,0) CNT composites is composed by the PIDT-BT components, while the LUMO is localized onto the (9,9) (12,8)(18,0) CNT. The DOS illuminates that states of PIDT-BT and (9,9) (12,8)(18,0) CNT mix well near the bottom of conduction band (CB), while the states close to the top of valence band (CB) are separated each other. The behavior reveals the coupling with CB states is stronger than VB states, account for the significant electron transfer from PIDT-BT to (10,2) CNT even without covalent linking between them. The HOMO and LUMO located separately on two species, which is beneficial for charge separation across the interface

In the case of PIDT-BT/(9,9) (12,8)CNT composites mix well near the bottom of conduction band (CB) than that of the (18,0), which indicate the donor–acceptor coupling; while in the case of PIDT-BT/(12,8)(18,0) CNT composites band gap between LUMO and HOMO is lower than that of PIDT-BT/(9,9) CNT composites, which reveal the low energy of electron transfer between LUMO and HOMO.

The PIDT-BT/(12,8)CNT composites show the coupling of two LUMOs near Fermi level, which is contributed to the probability of MEG of semi-conductive single wall carbon nanube due to the strongest Coulomb interactions , which show the best performance in electron separation.

Multiple exciton Generation of SWNT

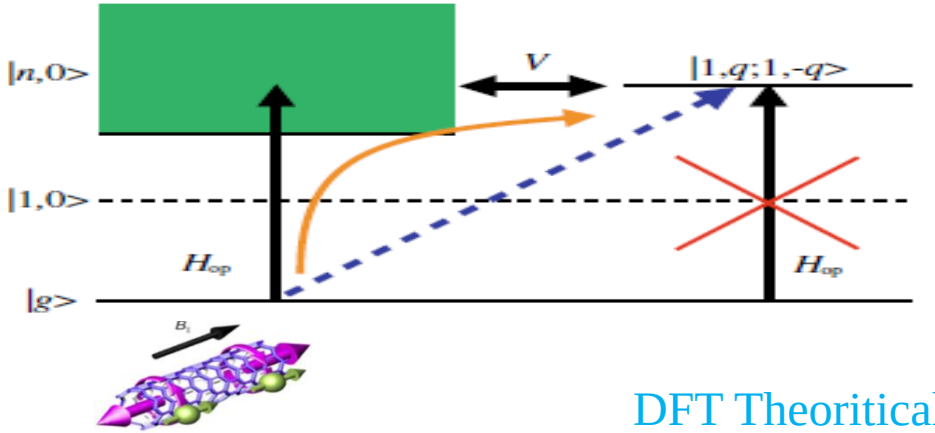

$$\Gamma_{\mathrm{MEG}}(\omega) = \frac{2\pi}{\hbar}\sum_{q}\left|\sum_{n}\frac{\langle g|\mathcal{H}_{\mathrm{op}}|n,0\rangle\langle n,0|V|1,q;1,-q\rangle}{E_q^1 + E_{-q}^1 - E_0^n + i\gamma}\right|^2 \times \delta(\hbar\omega - E_q^1 - E_{-q}^1). \quad (3)$$

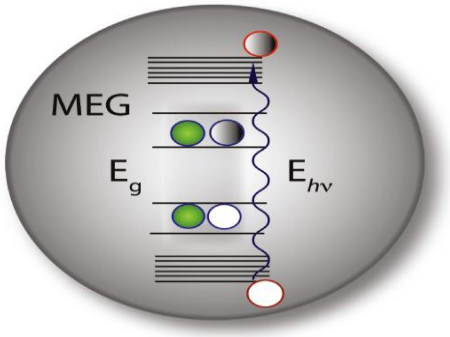

DFT Theoritical calculation has demonstrated that it is possible to generate two excitons by a single photon due to resonant coupling between the optically active one-exciton state and two exciton states. This resonance is ascribed to the unique characteristics of SWNTs that originate from their quasione-dimensional structures, resulting in a strong Coulomb interaction between excitons competing with phonon dephasing and the van Hove singularity in the density of states of the two-exciton states.

Heterjuction of conjugated polyme rand SWNT

quantum dot excited

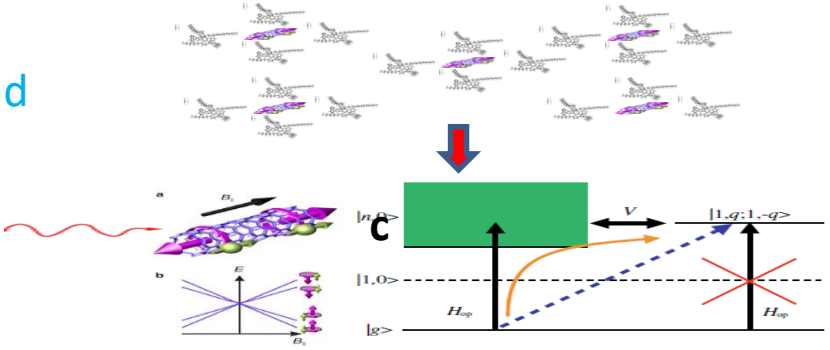

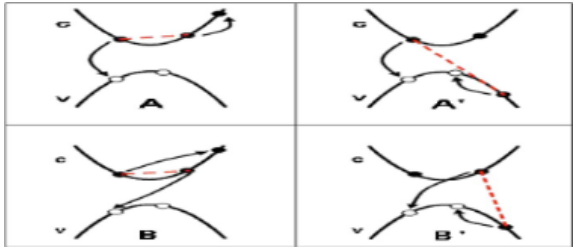

Rate of MEG

MEG

Auger recombination

$$\Gamma_{MEG}(\omega) = \frac{2\pi}{\hbar}\sum_{q}\left|\sum_{n}\frac{\langle g|\mathcal{H}_{op}|n,0\rangle\langle n,0|V|1,q;1,-q\rangle}{E_q^1 + E_{-q}^1 - E_0^n + i\gamma}\right|^2 \times \delta(\hbar\omega - E_q^1 - E_{-q}^1)$$

Rate of Auger Recombination

$$\Gamma_{Auger} = \frac{A}{L}\cdot N(N-1) \approx= 128\frac{\omega_{vc}}{k_{e0}}\cdot\left(\frac{\mu}{m_0}\right)\left(\frac{E_b}{E_g}\right)^3\cdot L\cdot n^2$$

Dissipation and sepaaration of exciton and transport of carriers

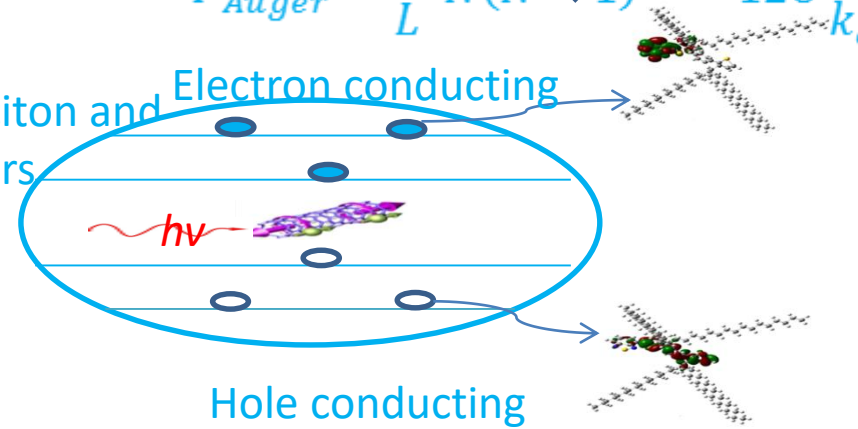

4 Conclusion

1 As the diameter of CNT increase, the distance between CNT and main chain of conjugated polymer decrease, but if the diameter of CNT is sufficient big, the conjugated polymer insert inside of CNT.

2 Multiple exciton generation of semi-conductive Single walled Carbon nanoutbe is a promising approach to increase internal quantum efficiencies to exceed unity for photon energies above the first direct band gap

3 The key to form helical structure of Conjugated polymer upon carbon nanotube heterojunction heterogeneous π complexes is the constructing of interfaces of conjugated polymer wrapping around CNT by self-assembly

4 The interfaces between PIDT-BT and single wall carbon nanotubes play a dominant role in the Nanostructure architecture of Conjuagted polymer/carbon nanotube, which is crucial to the tailor the competition between MEG and Auger recombination and improve the charge separation.

$$\Gamma_{MEG}(\omega) = \frac{2\pi}{\hbar}\sum_q \left| \sum_n \frac{\langle g|\mathcal{H}_{op}|n,0\rangle\langle n,0|V|1,q;1,-q\rangle}{E_q^1 + E_{-q}^1 - E_0^n + i\gamma} \right|^2 \times \delta(\hbar\omega - E_q^1 - E_{-q}^1)$$

$$\Gamma_{Auger} = \frac{A}{L}\cdot N(N-1) \approx= 128\frac{\omega_{vc}}{k_{e0}}\cdot\left(\frac{\mu}{m_0}\right)\left(\frac{E_b}{E_g}\right)^3\cdot L\cdot n^2$$

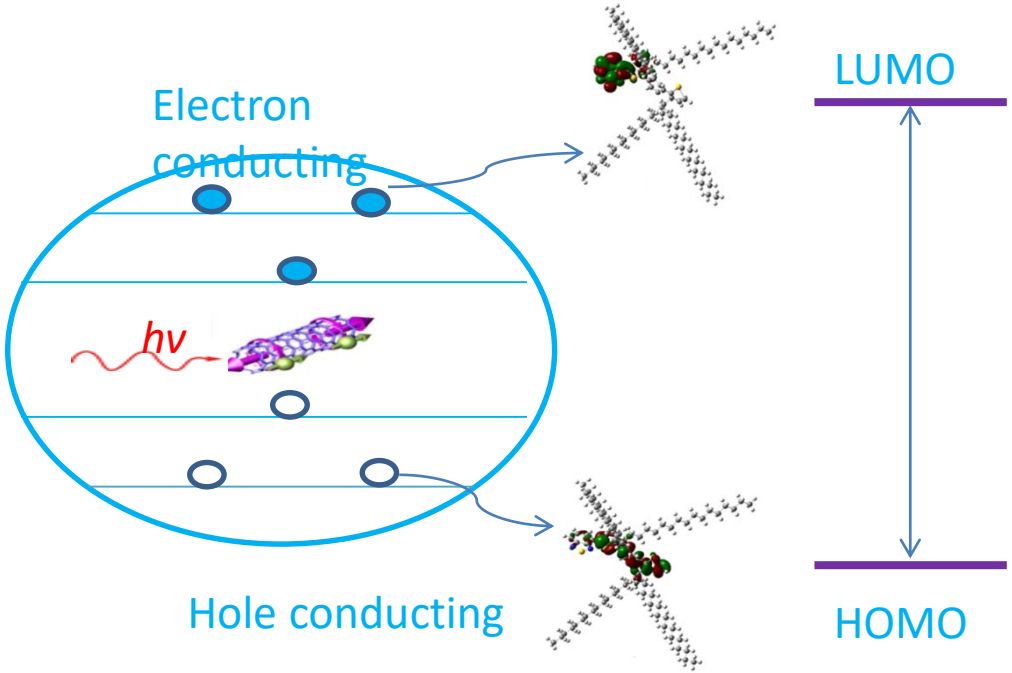

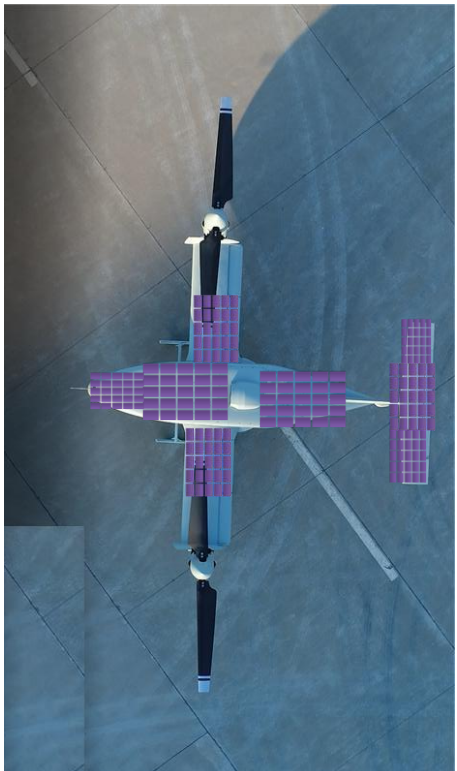

plan

- What's the fundamental mechanism responsible for the MEG process of single wall carbon nanotube are currently open questions.
- Experiemtns:
- 1 both conjugated polymer and single walled carbon nanotube can play as quantum dot alone
- 2 prepare heterogeneous complexes of conjugated polymer and carbon nanotube
- 3 nanostructure of the complexes
- 4 photon-electron conversion study of the complexes

Thanks for your attention

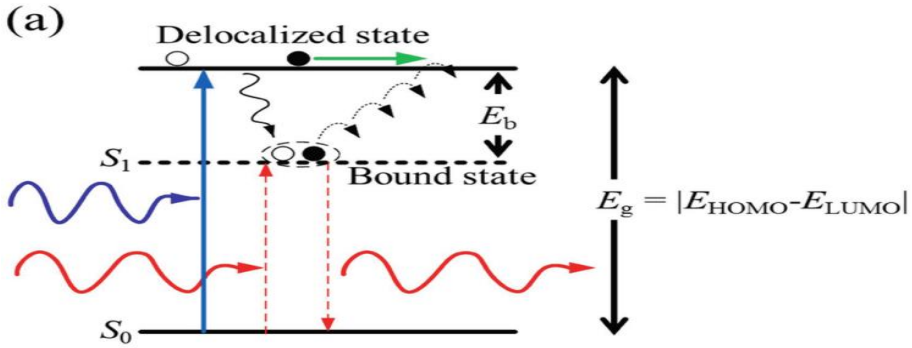
(a)
Delocalized state
E_b
S_1
Bound state
$E_g = |E_{HOMO}\text{-}E_{LUMO}|$
S_0

(b)

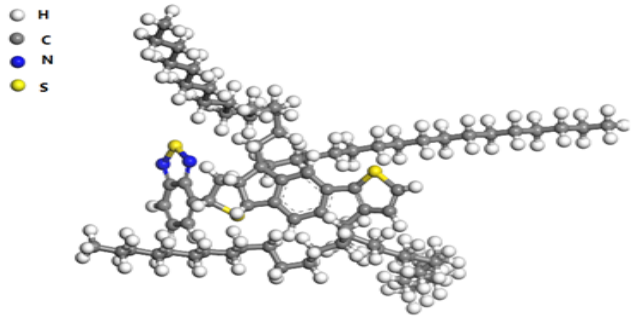
H
C
N
S

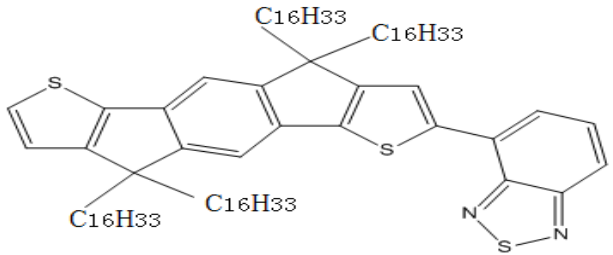
C16H33
C16H33
S
S
C16H33
C16H33
N
S
N

（a）

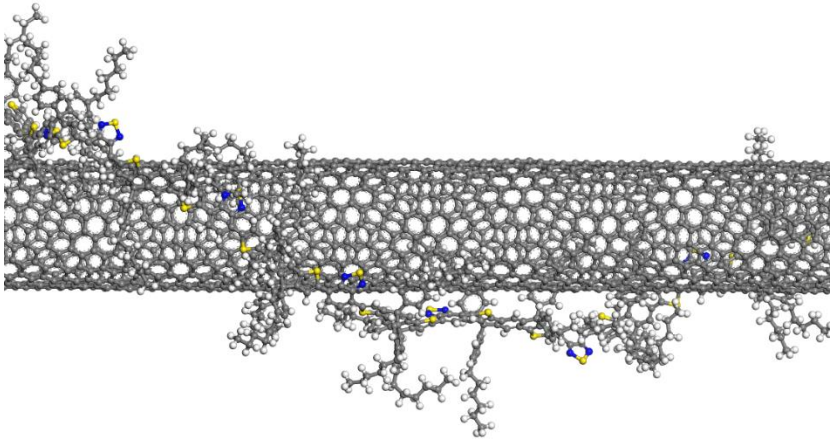

（b）

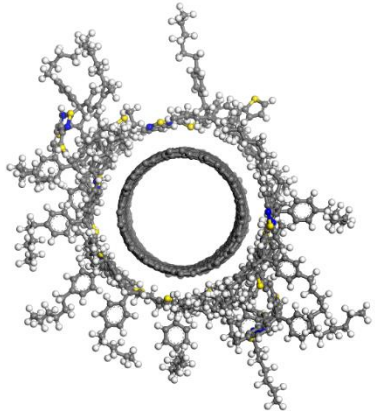

（a）

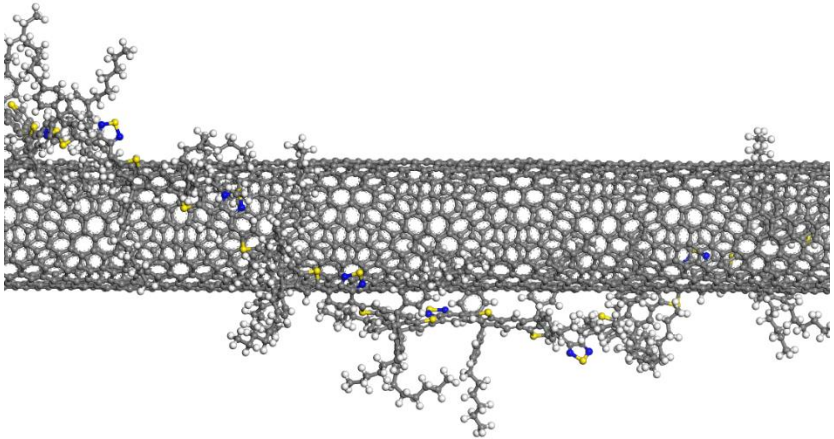

（b）